

## Local field potential activity dynamics in response to deep brain stimulation of the subthalamic nucleus in Parkinson's disease

C. Wiest<sup>a,b</sup>, G. Tinkhauser<sup>c</sup>, A. Pogosyan<sup>a,b</sup>, M. Bange<sup>d</sup>, M. Muthuraman<sup>d</sup>, S. Groppa<sup>d</sup>, F. Baig<sup>a,b,e</sup>, A. Mostofi<sup>e</sup>, E.A. Pereira<sup>e</sup>, H. Tan<sup>a,b</sup>, P. Brown<sup>a,b</sup>, F. Torrecillos<sup>a,b,\*</sup>

<sup>a</sup> Medical Research Council Brain Network Dynamics Unit, University of Oxford, Oxford, UK

<sup>b</sup> Nuffield Department of Clinical Neurosciences, John Radcliffe Hospital, University of Oxford, Oxford, UK

<sup>c</sup> Department of Neurology, Bern University Hospital, Bern, Switzerland

<sup>d</sup> Movement Disorders and Neurostimulation, Biomedical Statistics and Multimodal Signal Processing Unit, Department of Neurology, Mainz University Hospital, Mainz, Germany

<sup>e</sup> Neurosciences Research Centre, Molecular and Clinical Sciences Institute, St. George's, University of London, London, UK

### ARTICLE INFO

#### Keywords:

Parkinson's disease  
Local field potentials  
Evoked resonant neural activity  
Beta oscillations  
High frequency oscillations  
Gamma activity  
Adaptive deep brain stimulation  
Feedback markers

### ABSTRACT

Local field potentials (LFPs) may afford insight into the mechanisms of action of deep brain stimulation (DBS) and potential feedback signals for adaptive DBS. In Parkinson's disease (PD) DBS of the subthalamic nucleus (STN) suppresses spontaneous activity in the beta band and drives evoked resonant neural activity (ERNA). Here, we investigate how STN LFP activities change over time following the onset and offset of DBS. To this end we recorded LFPs from the STN in 14 PD patients during long (mean: 181.2 s) and short (14.2 s) blocks of continuous stimulation at 130 Hz. LFP activities were evaluated in the temporal and spectral domains. During long stimulation blocks, the frequency and amplitude of the ERNA decreased before reaching a steady state after ~70 s. Maximal ERNA amplitudes diminished over repeated stimulation blocks. Upon DBS cessation, the ERNA was revealed as an under-damped oscillation, and was more marked and lasted longer after short duration stimulation blocks. In contrast, activity in the beta band suppressed within 0.5 s of continuous DBS onset and drifted less over time. Spontaneous activity was also suppressed in the low gamma band, suggesting that the effects of high frequency stimulation on spontaneous oscillations may not be selective for pathological beta activity. High frequency oscillations were present in only six STN recordings before stimulation onset and their frequency was depressed by stimulation. The different dynamics of the ERNA and beta activity with stimulation imply different DBS mechanisms and may impact how these activities may be used in adaptive feedback.

### 1. Introduction

Deep brain stimulation (DBS) has proven a successful treatment for advanced Parkinson's Disease (PD) since it was pioneered by Alim-Louis Benabid in 1987 (Lozano et al., 2019; Okun, 2012). Since then the paradigm has remained relatively unchanged and comprises continuous high-frequency stimulation delivered at a fixed frequency (usually 130 Hz) to either the subthalamic nucleus (STN) or the internal globus pallidus (GPi). Despite its success, the mechanisms of action of DBS remain largely unexplained (Muthuraman et al., 2018). This is important as DBS can elicit stimulation-related side effects that include speech impairment, neuropsychiatric symptoms and paradoxical worsening of motor functions (Chen et al., 2006a; Okun, 2012; Parsons et al., 2006). An understanding of the mechanisms of action of DBS

could enable development of DBS strategies that are more specific, causing fewer side-effects, and even more effective, should it prove possible to directly counter the key malfunctions in neural circuits. In particular, there has been much recent interest in the possibility of controlling DBS using feedback from electrophysiological signals (Bouthour et al., 2019; Little and Brown, 2020; Lozano et al., 2019).

In order to clarify the mechanisms of action of DBS and seek suitable feedback signals it makes sense to examine the effects of DBS on neural circuits at the point of stimulation. Thus far two major direct consequences of stimulation have been identified in the STN; the suppression of beta-band activity in the local field potential (LFP) and the stimulation evoked resonant neural activity (ERNA; Sinclair et al., 2018). The former has been suggested as a potential mechanism underlying effective DBS, based on the growing evidence that Parkinson's

\* Corresponding author at: Nuffield Department of Clinical Neurosciences, University of Oxford, Level 6, West Wing, John Radcliffe Hospital, Oxford OX3 9DU, UK.  
E-mail address: [flavie.torrecillos@ndcn.ox.ac.uk](mailto:flavie.torrecillos@ndcn.ox.ac.uk) (F. Torrecillos).

<https://doi.org/10.1016/j.nbd.2020.105019>

Received 22 May 2020; Received in revised form 17 June 2020; Accepted 11 July 2020

Available online 16 July 2020

0969-9961/ © 2020 The Authors. Published by Elsevier Inc. This is an open access article under the CC BY-NC-ND license (<http://creativecommons.org/licenses/by-nc-nd/4.0/>).

disease is associated with exaggerated synchronisation of basal ganglia neurons in the beta frequency band (13–35 Hz; Brown, 2003; Eusebio et al., 2011; Kühn et al., 2008; Quinn et al., 2015). The ERNA has been more recently reported, and can be described as a robust, decaying, large-amplitude and high-frequency oscillation following DBS pulses (Sinclair et al., 2018, 2019b). It has been confirmed to be of neural origin and is modulated by changes in DBS parameters, although its relationship to DBS mechanisms has barely been explored (Sinclair et al., 2019a).

The ERNA and beta activity are quite different, not least in their amplitudes, and yet both have been suggested as possible feedback signals to be used in adaptive DBS given evidence that they may correlate with motor impairment (Kühn et al., 2006; Kühn et al., 2009; Little et al., 2013; Sinclair et al., 2018). Here, we aim to investigate the responses of these two activities to high-frequency stimulation of the STN with special reference to the temporal dynamics of their responses. Our findings suggest that the different responses of the two activities may provide a window into different mechanisms underlying the effects of DBS of the STN whilst also constraining their use as feedback parameters in adaptive DBS.

## 2. Materials and methods

### 2.1. Patients and surgery

Fourteen patients with PD (two females) undergoing bilateral STN-DBS surgery participated in the study. Their mean age at the time of the recording was  $58 \pm 1.7$  years (mean  $\pm$  SEM) with average disease duration of  $11.2 \pm 1.1$  years. Patients were recruited at St. George's University Hospital NHS Foundation Trust, London (UK) and at the University Medical Center of the Johannes Gutenberg University, Mainz (DE) and they all gave their written informed consent to participate in the experiment approved by the local ethics committees (St. George's University Hospital, IRAS: 46576; Mainz University Hospital: 837.208.17(11042)). The clinical details of the patients are reported in Table 1 along with details of the surgical interventions and recordings (Table 2). UPDRS Part III scores were determined pre-operatively.

The implanted leads were the Medtronic 3389 (Medtronic Inc., Neurological Division, USA) with four 0.5 mm spaced contacts of 1.5 mm length with platinum-iridium cylindrical surfaces, or the directional leads from Boston Scientific (model DB-2202, Boston Scientific, USA) or St. Jude Medical (model 6170, St. Jude Medical, now Abbott, USA), both having three segmented contacts on the middle levels. DBS implantation was guided either by magnetic resonance imaging alone (St. George's University Hospital) or with additional intra-operative micro-recordings and intra-operative stimulation (University Medical Center, Mainz).

### 2.2. Stimulation and data recording

Recordings were made between 2 and 5 days postoperatively (Table 2), while electrode leads were still externalised and before implantation of the subcutaneous pulse generator. All patients performed the experiments after overnight withdrawal of antiparkinsonian medication. For the patients implanted with directional leads, the directional contacts of levels 1 and 2 were joined together to form one 'ring contact' so that each lead afforded four monopolar ring contacts. The four contacts were then numbered from E0 to E3 with contact 0 being the most ventral and contact 3 being the most dorsal (see Fig. 1A). Stimulation was only tested at the two middle contacts (E1 and E2) to allow bipolar LFP recordings from the two adjacent contacts (see end of this paragraph and Fig. 1A). A self-adhesive electrode (Pals, Nidd Valley Medical, Bordon, UK) attached to the back of the participants' shoulders served as reference for the stimulation, which was delivered using a highly configurable neurostimulator (Slater et al., 2015). Stimuli comprised symmetric constant-current biphasic pulses (60  $\mu$ s per phase,

**Table 1**

Patients clinical details. Pre-op: Preoperative. UPDRS-III: Part III motor score of the Unified Parkinson's Disease Rating Scale. The last three cases had no evidence of an ERNA (see Table 2).

Sub.	Gender (m/f)	Age (yr)	Disease Duration (yr)	Pre-OP UPDRS-III OFF	Pre-OP UPDRS-III ON	Pre-dominant symptoms
1	m	61	16	50	30	Gait freezing, motor fluctuations
2	m	48	17	71	37	Rigidity, tremor, gait freezing
3	m	54	7	38	24	Tremor
4	m	56	16	51	19	Rigidity, bradykinesia
5	m	65	5	34	16	Gait freezing, motor fluctuations
6	m	51	5	27	13	Bradykinesia, rigidity, motor fluctuations
7	f	63	11	40	17	Gait freezing, motor fluctuations
8	m	64	13	52	21	Gait freezing, motor fluctuations
9	m	61	10	31	19	Akinetic-rigid, tremor
10	m	61	11	16	7	Akinetic-rigid with fluctuations
11	m	53	7	23	12	Tremor
12	m	61	9	33	12	Right arm tremor, bradykinesia
13	m	48	8	45	34	Tremor, bradykinesia
14	f	67	13	18	15	Akinetic-rigid, tremor

negative phase first). For each of the two contacts, stimulation was started at 0.5 mA and slowly increased by 0.5 mA increments every 3 to 4 min until a clear clinical benefit in rigidity and/or bradykinesia was observed or side effects such as paresthesia became apparent. The stimulation contact and current associated with the most clinically effective stimulation without side effects was then selected and maintained for the entire experiment (Table 2). This procedure was performed on the side contralateral to the most affected upper limb in 12 subjects and bilaterally in 2 subjects. A stimulation frequency of 130 Hz was used throughout.

Signals were amplified and sampled at 2048 Hz using a TMSi Porti and its respective software (TMS International, Netherlands). STN LFPs were recorded bipolarly from the two contacts either side of the contact used for stimulation, for common reference removal (Schiff, 2005). The ground electrode was placed on the forearm.

### 2.3. Lead localisation determination

Assessment of contact localisation was made through co-registration of immediate post-operative CT with pre-operative MRI by an experienced neurosurgeon (E.A.P) or neurologist (S.G.) specialising in deep brain stimulation. Assessment was blinded to the electrophysiological data and made using Renishaw Neuroinspire v6 software in London and Lead-DBS (v2.0, Horn et al., 2019) in Mainz. These assessments are summarised in Table 2.

### 2.4. Experimental protocol

During the experiment, patients were seated comfortably in an armchair. The experimental protocol is summarised in Fig. 1B and consisted of two conditions preceded by 2 min of rest recordings without stimulation (baseline). In the first condition, continuous 130 Hz DBS was applied for  $181.2 \pm 7.3$  s (mean  $\pm$  SEM) in up to four consecutive blocks separated by resting periods of on average

**Table 2**

**Patients surgical and recordings details.** Medt: Medtronic. L: Lef., R: Right. STN(SP): Superior posterior part of sub-thalamic nucleus. MBSTN(SP): Medial border of the superior posterior part of the sub-thalamic nucleus. Post lat to STN (SP): Posterio-lateral to the superior posterior part of the sub-thalamic nucleus. D: ERNA during stimulation, A: ERNA after stimulation. Incl: STN included in the power analysis of local field potentials (LFP, beta and low gamma power). Mvt art: STN excluded from LFP power analysis because of movement artefacts. Beta red: beta reduced. \* only two blocks of which were consecutive (patients excluded from linear mixed-effects models).

Sub.	DBS lead	Site	Time Recording (d)	STN tested	Location Stim. Contact	Stim. Amp. (mA)	Cond.	no. of blocks in cond. 1	ERNA	LFP Power analysis
1	Boston	St. George's London	3	L	STN (SP)	2	1,2	4	D,A	Incl.
2	Boston	St. George's London	4	R	STN (SP)	2	1	4	D	Mvt art.
3	Boston	St. George's London	5	R	STN (SP)	3,5	1	4	D,A	Incl.
4	Medt	St. George's London	4	L	STN (SP)	4	1	4	D,A	Incl.
5	Boston	St. George's London	4 and 5	L	MBSTN (SP)	3	1,2	3	D,A	Incl.
			4	R	MBSTN (SP)	2,5	1,2	3	D,A	Incl.
6	Boston	St. George's London	4	R	MBSTN (SP)	4	1	4	D	Mvt art.
7	Boston	St. George's London	4	L	STN (SP)	2	1,2	3*	D,A	Incl.
8	Boston	St. George's London	4	R	STN (SP)	2	1,2	3*	D,A	Incl.
9	Medt	University Medical Center, Mainz	3	L	STN (SP)	4	1	4	D,A	Incl.
10	St. Jude	University Medical Center, Mainz	2	R	STN (SP)	3,5	1	4	D,A	Incl.
11	Boston	St. George's London	4	R	STN (SP)	2	1,2	4	D,A	Incl.
			5	L	STN (SP)	3	1,2	4	D,A	Incl.
12	Boston	St. George's London	4	L	MBSTN (SP)	4	1	4	none	Beta red.
13	Boston	St. George's London	5	L	MBSTN (SP)	3	1	4	none	No beta change
14	Medt	University Medical Center, Mainz	3	L	Post lat to STN(SP)	1,5	1	4	none	Beta red.

117.1  $\pm$  10.8 s. These are termed long duration stimulation blocks. In the second condition, stimulation blocks were shortened to on average 14.2  $\pm$  2.3 s with rest periods of 105.1  $\pm$  16 s. This second condition was performed to study how the ERNA's characteristics are modulated by the duration of the preceding stimulation and both conditions were separated by a resting period. In addition, the long duration stimulation condition was long enough for clinical benefit to develop (Levin et al., 2009; Lopiano et al., 2003). The rest period duration did not differ between the two conditions ( $t_{(18)} = 0.55, p = .59$ ). Note that due to patient fatigue and time constraints only a subset of patients performed the short duration condition ( $n = 7$  STN from 5 patients).

#### 2.4.1. Terminology

The ERNA has previously only been described in the temporal domain, with the same term being used to describe evoked responses during and at the termination of stimulation (Sinclair et al., 2018, 2019b). Here we also use the term ERNA to describe a feature in time-frequency plots that upon steady-state has a similar frequency to the repeating waves of the ERNA on cessation of stimulation. Time and spectral domain representations also shared similar dynamics following the onset of stimulation. Hence we use the term ERNA to denote all three phenomena; the high frequency evoked response in time series during stimulation, the high frequency response in time series evoked by the last stimulus in a block of stimulation and the high frequency spectral response during stimulation.

#### 2.5. Signal processing: DBS evoked response

Signal processing was performed using custom-written scripts in MATLAB (version 2019a, Mathworks, Massachusetts, USA).

#### 2.6. ERNA during stimulation

Here, we determine ERNA characteristics in the frequency domain, based on the premise that the ERNA is not sufficiently tuned as to be wholly obscured by the stimulation artefact in frequency spectra. These analyses were performed only during long stimulation blocks (condition 1). Continuous LFP signals were de-trended and stimulation artefacts were removed by applying second-order IIR notch filters ( $Q$  factors = 30) at the stimulation frequency and its harmonics. Spectral amplitudes were estimated between 1 and 512 Hz using the short-time Fourier transform with a window length of 1 s, 25% of overlap and a Hamming window as implemented in MATLAB's *spectrogram* function (see Fig. 1C for data from one STN). Each long stimulation block (condition 1) was then divided into consecutive non-overlapping 10-s epochs, in which power spectral densities (PSD) were estimated and smoothed using a Gaussian kernel with 50 sampling points full-width. The largest peak of the PSD between 200 and 400 Hz was used to define the ERNA frequency and amplitude in each 10-s epoch (see Fig 2Aii and Supplementary video V1). Based on the changes observed along the consecutive 10-s epochs we then separately defined for each long duration stimulation block two steady states corresponding to the stabilisation of the ERNA frequency (Fig 2Aiii) and amplitude (Fig 2Aiv), respectively. The onset of the steady state was defined based on the derivative of the time profiles and corresponded to the centre of the first epoch at which the derivative was encompassed in a band of  $\pm 5$  Hz/s (or  $\mu$ V/s for amplitude) centred around zero. This method allowed a robust and objective threshold estimation while limiting the number of arbitrary selected parameters.

The spectral analysis of the ERNA during continuous stimulation was supported by its analysis in the time domain. To this end, the peaks of the stimulation artefacts were identified and removed from the de-

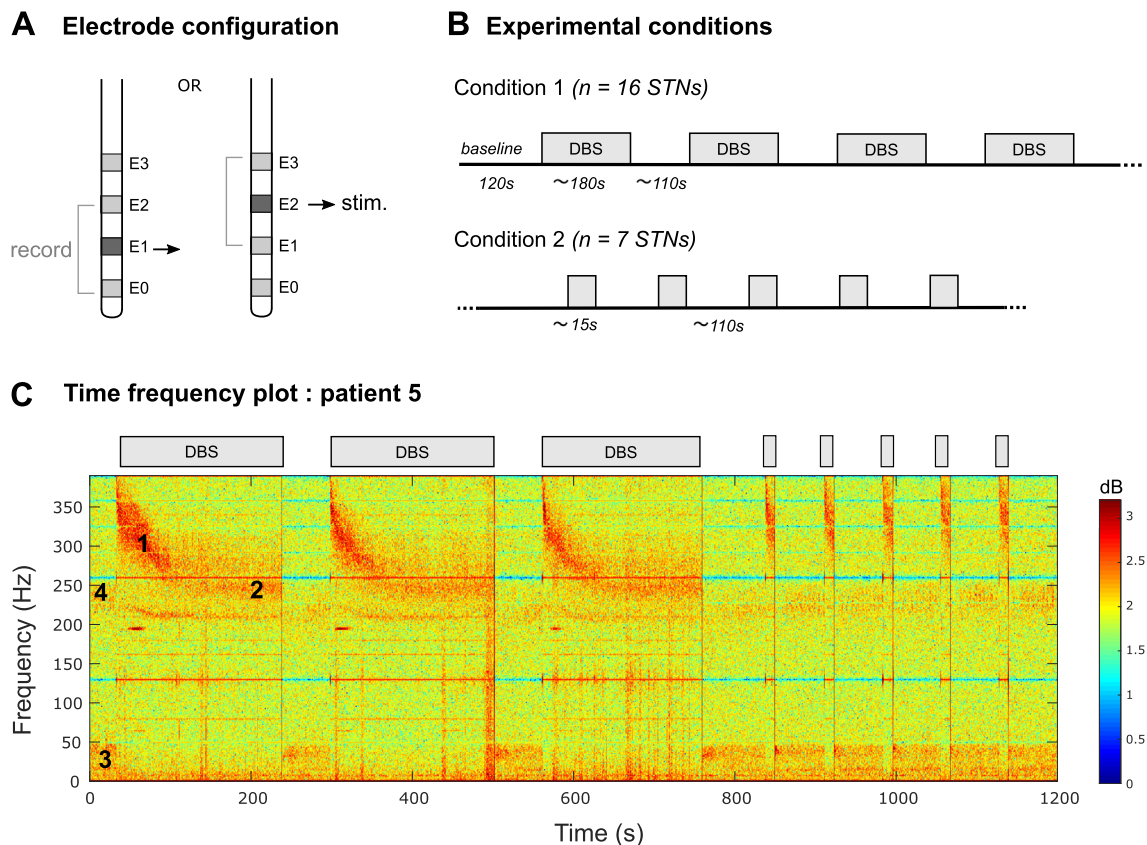


**Fig. 1.** Stimulation settings and experimental conditions. **A.** Schematic of the electrode configuration. Stimulation was applied to one of the two middle electrode contacts (E1 or E2) and the LFPs recorded bipolarly from the two adjacent contacts (e.g.: E1-E3). **B.** Experimental protocol. The first condition started with a 2-min baseline recording followed by continuous stimulation at 130 Hz in blocks of  $181.2 \pm 7.3$  (mean  $\pm$  SEM) seconds interleaved by about  $117.1 \pm 0.8$  s of rest. In the second condition, stimulation was shortened to  $14.2 \pm 2.3$  s and separated by about  $105.1 \pm 16$  s. Rest period duration did not differ between the two conditions ( $t_{(18)} = 0.55$ ,  $p = .59$ ). **C.** Spectral features over time in the two experimental conditions for patient 5. During stimulation, an ERNA appears between 300 Hz and 350 Hz (label 1) and its power attenuates while dropping in frequency until it reaches a steady state centred around 260 Hz (label 2). Stimulation blocks are denoted by the grey rectangles at the top of the trace. In addition, during stimulation there is a prompt suppression of beta and low gamma power (label 3) and a modulation of the HFO frequency (label 4) present before stimulation. Note that line noise artefacts are visible throughout the recordings at 50 Hz and its harmonics, along with the stimulation artefact at 130 Hz and its harmonics, despite being reduced by notch filters. Movement artefacts, affecting mostly lower frequencies, are particularly visible in the third stimulation block.

trended LFP signals (removing 1.5 ms after each artefact to avoid any contamination of the inter-trial interval by residual stimulus artefact). Note that 1.5 ms was selected as sufficient to remove stimulus artefact based on visual inspection. Then, the first ERNA peak was identified in the inter-artefact intervals ( $\sim 7.7$  ms long) of the stimulation block as the highest peak within the interval, and tracked throughout all consecutive intervals to measure its amplitude and latency (time between artefact peak and first peak of the ERNA).

## 2.7. ERNA after stimulation

After cessation of stimulation the ERNA was assessed over a longer time window which exposed its extended morphology characterised by a series of 2–8 regularly spaced, but diminishing waves (Sinclair et al., 2018, 2019b). The ERNA after stimulation was analysed as follows. First, data were high-pass filtered at 80 Hz with a two-pass Butterworth IIR filter (Oostenveld et al., 2011) and 50 ms data epochs were aligned to the last reproducible stimulus artefact in a given block of stimulation. ERNA duration was defined as the time between the last artefact peak and the last detected ERNA peak within the 50-millisecond epoch. Thereafter, the first 1.5 ms of each epoch was deleted to avoid further contamination by residual stimulus artefact (see Fig. 4A). Second, peaks and troughs in the ERNA response were found using the MATLAB *findpeaks* function, with the following criteria;

MinPeakWidth = 0.5 ms, MinPeakProminence =  $10 \mu\text{V}$  (Sinclair et al., 2019b). ERNA responses were not further analysed, and considered absent, if there were fewer than two peaks and two troughs. Finally, ERNA initial frequency was calculated as the inverse of the time difference between the first and second peak and the initial amplitude was calculated as the difference between the first peak and the subsequent trough (Sinclair et al., 2019b). To evaluate the ERNA frequency change after cessation of the stimulation, its frequency was also calculated as the inverse of the time between the subsequent peaks.

## 2.8. Signal processing: spontaneous neural activity

### 2.8.1. Lower frequency band (1–95 Hz)

LFP signals were band-pass filtered between 1 and 95 Hz and spectra were estimated using the short-time Fourier transform with a higher temporal resolution than for the previous analysis (window length of 125 ms, 50% of overlap) and a Hamming window filter. All spectral power changes were defined in relation to a 10-s baseline epoch recorded prior to the first stimulation block of every subject which was free from any motion artefact. The modulation of resting, spontaneous beta (13–34 Hz) and low gamma (35–45 Hz) power by DBS was studied in two 30-s windows aligned to the first and last artefact in long duration stimulation blocks (from  $-10$  to  $+20$  s where zero seconds is the onset and offset of stimulation, respectively). For

both frequency bands, the time of power recurrence was defined after the cessation of stimulation as an increase in power that reached or surpassed the 95% confidence limits of baseline activity for at least 250 ms. For clinical correlations baseline beta power was normalised to the percentage of total power of 5 to 45 Hz.

### 2.8.2. High Frequency Oscillations (HFO, 200–400 Hz)

Spontaneous activity in the high frequency range (200–400 Hz) was studied in the absence of stimulation, as it can overlap with the frequency range of the evolving ERNA. Power spectral densities were estimated using MATLAB's *spectrogram* function (same parameters as for the ERNA during DBS) in 20-s windows during the baseline and at the start or end of the resting periods (see Fig. 7A). In each window, the HFO frequency peak was defined as the largest peak between 200 and 400 Hz.

## 2.9. Statistics

The statistical analyses were conducted using custom-written scripts in MATLAB (MathWorks). Normality of the data was controlled before any statistical test (Lilliefors test) and nonparametric statistics were applied when necessary (as reported in Results). Comparison of group data (ERNA characteristics and averaged power changes) across stimulation blocks were performed with linear mixed-effects models and the normal distribution of each variable was visually inspected with quantile-quantile plots and histograms of distribution. All models were estimated by the method of maximum likelihood and included random intercept for subjects, to allow different intercepts for each subject capturing individual differences. The time courses of power changes were tested against zero with one-sample *t*-tests in sliding windows of 50 ms with a time shift between successive windows of 12.5 ms. The False Discovery Rate was computed using the Benjamini-Hochberg procedure (Benjamini and Hochberg, 1995) to correct for multiple comparisons along the time axis. Since power data are not normally distributed and contain outliers, we computed the Spearman correlation between suppression of activity in the beta band, time to reach ERNA steady state and symptom severity.

## 3. Results

### 3.1. ERNA during stimulation

We began by inspecting time-frequency plots of STN activity during stimulation. A typical example from a representative patient is illustrated in Fig. 1C and shows, in the spectral domain, an activity sliding down in frequency over time before overlapping with the narrower band artefact at 260 Hz related to the first harmonic of the stimulation. This pattern was observed in 13/16 tested STNs. Here we term this activity ERNA based on its similarities to the ERNA previously described in the time-domain (see Fig. 3 and Sinclair et al., 2019b, 2018). Note that the absence of ERNA in three STNs is unlikely to be due to a weaker stimulation amplitude (see Table 2 and Fig. S1). Rather it may be related to targeting in so far as their stimulating contacts were localized to the medial border of the superior part of the STN or lay outside and postero-lateral to this part of the STN (see Table 2).

In order to study the frequency dynamics of the ERNA in more detail we divided each stimulation block into consecutive 10-s windows and plotted the peak frequency observed between 200 and 400 Hz over time (see Fig. 2A and Supplementary video V1). We then extracted three parameters for each stimulation block: the initial and steady state frequencies, and the time at which the steady state was reached (see Methods). We first asked whether the three parameters were consistent over time, i.e. across stimulation blocks. To this end we only considered those patients with at least three consecutive long duration stimulation blocks ( $n = 11$  STNs, including seven with four blocks). The results of linear mixed-effects modelling revealed that both the initial and steady

state frequencies were stable over long duration stimulation blocks ( $b = -0.45$ ,  $t_{(38)} = -0.37$ ,  $p = .72$  and  $b = 0.49$ ,  $t_{(38)} = 1.27$ ,  $p = .21$ , respectively, Fig. 2B). Moreover, the delay to reach the steady state was also similar in consecutive blocks ( $b = -2.48$ ,  $t_{(38)} = -1.86$ ,  $p = .07$ ). Thus, on average across all STNs and stimulation blocks, the ERNA started at a frequency of  $352.4 \pm 4.9$  Hz (mean  $\pm$  SEM) at the onset of stimulation and progressively decreased in frequency over time to stabilise after  $71.4 \pm 2.6$  s at a frequency of  $263.2 \pm 2.1$  Hz.

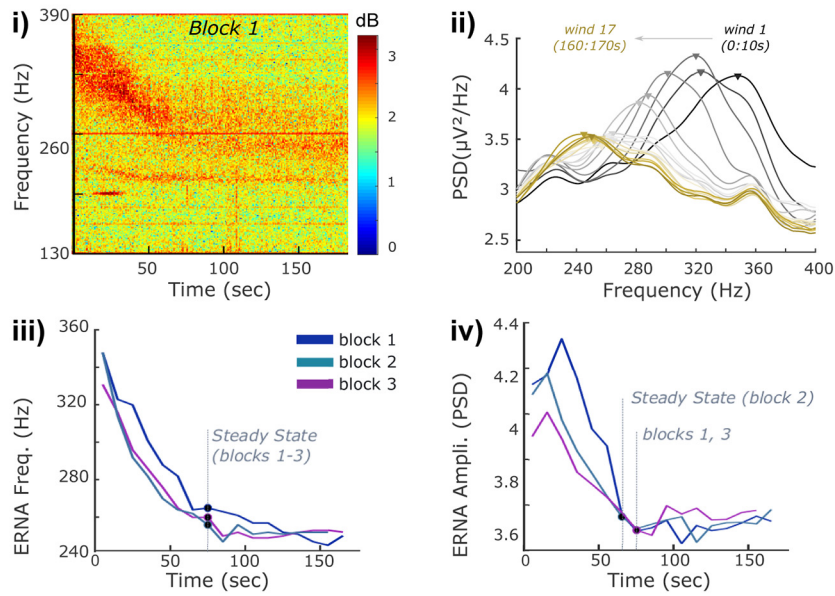
In addition to the dynamics in frequency, we also explored the dynamics in the ERNA amplitude, following the same procedure. As shown in Fig. 2Aiv and 2C, the results revealed a different pattern. The amplitude of the evoked response first briefly increased and then decreased to stabilize around a steady state at the end of the stimulation block (after on average  $81.7 \pm 6.2$  s). For each STN and each stimulation block, we extracted five parameters describing this amplitude dynamic; the initial, maximal and steady state amplitude, and the times at which the maximal and steady state amplitudes were reached. The linear mixed-effects modelling revealed a significant reduction of the maximal amplitude and a shortening of the delay to reach the steady state in consecutive blocks ( $b = -0.06$ ,  $t_{(38)} = -3.56$ ,  $p = .013$  and  $b = -6.27$ ,  $t_{(38)} = -2.21$ ,  $p = .03$ , respectively). The results are confirmed when only the STNs with four consecutive blocks were included in the model (maximal amplitude:  $b = -0.06$ ,  $t_{(26)} = -2.68$ ,  $p = .013$  and steady state:  $b = -7.1$ ,  $t_{(26)} = -2.1$ ,  $p = .047$ ). This control was performed to confirm that the previously reported statistical effects were not related to the unbalanced design and the absence of block 4 in some of the STNs. This modulation can be easily seen in Fig. 2C bottom right where the amplitude time course of the first and last stimulation block are overlaid. The three remaining parameters were however stable in consecutive blocks; the time at which the maximal amplitude was reached ( $b = 0.21$ ,  $t_{(38)} = 0.07$ ,  $p = .94$ ) as well as the initial and steady state amplitudes ( $b = -0.004$ ,  $t_{(38)} = -0.26$ ,  $p = .8$  and  $b = 0.01$ ,  $t_{(38)} = 1$ ,  $p = .32$ , respectively). Finally, the frequency and amplitude steady states were reached after a similar delay (paired *t*-tests,  $t_{(12)} = -1.01$ ,  $p = .3$  for the first block,  $t_{(12)} = 0.17$ ,  $p = .87$  for the last block).

Importantly, the above results were confirmed by studying the ERNA during stimulation in the temporal domain (Fig. 3A). During continuous DBS the evoked response can be observed between each pair of consecutive stimulation artefacts, although it may also be present during the stimulus artefact but obscured by the latter (see Fig. 4C). In order to demonstrate the changing nature of the evoked activity over time we selected the maximal discrete peak between the stimulus artefacts. This increased in latency and decreased in amplitude with stimulation duration (Fig. 3B and Supplementary video V2) and is in line with the change in frequency and amplitude observed in the spectral domain (Fig. S2). Note that the latency of the selected peak may not exactly correspond to the frequency of the ERNA measured in the spectral domain, as in the latter case the analysis gives the dominant frequency of the whole evoked response, and may include portions of the evoked activity that overlap with the stimulation artefact (see Fig. 4C). The time-domain analysis also confirmed the absence of an ERNA during stimulation in the three patients mentioned previously (patients 12–14, Table 2, Fig. S1).

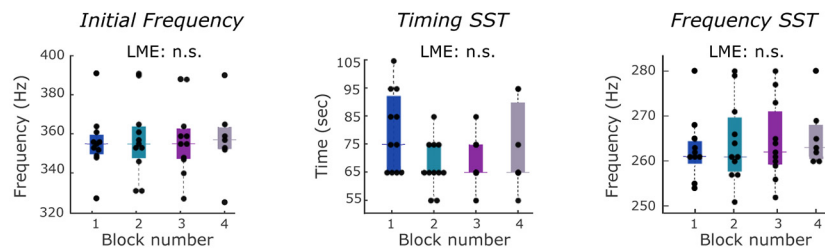
### 3.2. ERNA after stimulation

As mentioned above, time domain analyses of the ERNA during stimulation may be hindered by subsequent stimulation artefacts. Accordingly, we also examined any activity that persisted after stimulation was abruptly discontinued. As can be seen in Fig. 4A, a series of high frequency waves followed cessation of stimulation and progressively diminished in amplitude, similar to the ERNA previously described in the literature (Sinclair et al., 2018). Across all hemispheres, this resonant activity was composed of a series of 2 to 10 waves

## A Patient 5 : ERNA Frequency and Amplitude



## B Group Data : ERNA Frequency



## C Group Data: ERNA Amplitude

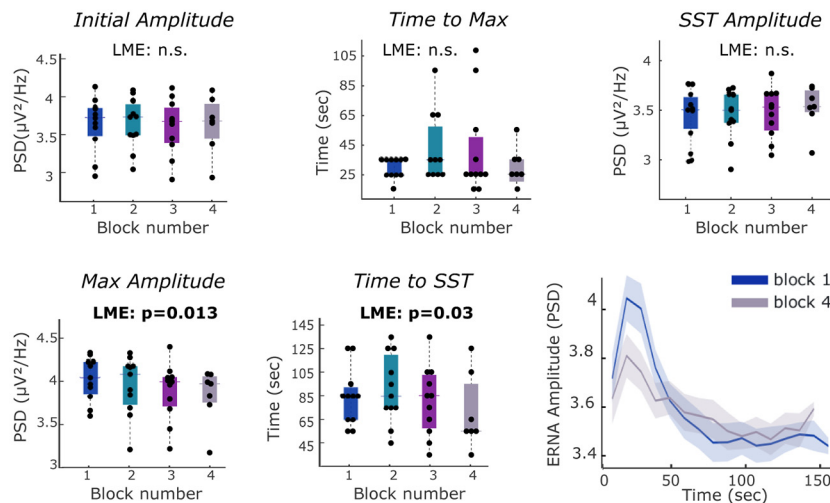


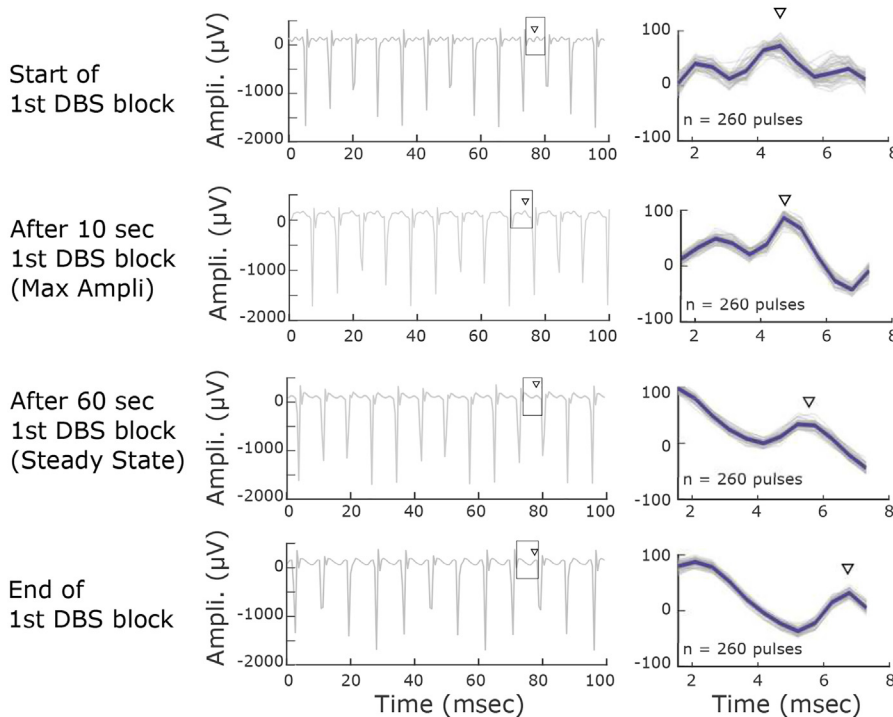
**Fig. 2.** ERNA during long stimulation blocks (condition 1) characterised in the spectral domain. **A.** ERNA in Patient 5. ERNA representation in a time-frequency plot (i) and power spectral density (PSD) in serial 10-s windows (wind;  $n = 17$ ) (ii). Successive windows transition from black to light grey and then to brown, showing the progression to steady state. The arrow heads denote the frequency of the peak measured in each window. The amplitude and frequency of this peak was measured to give the results in (iii) and (iv). The change in the ERNA frequency (iii) and amplitude (iv) over time are plotted for the three blocks of stimulation separately. The time at which steady state (SST) is reached corresponds to the first point at which the derivative remains within a  $\pm 5$  Hz/s band around zero and is indicated by dots for each block (see dashed grey line). **B.** Frequency characteristics of the ERNA at the group level and across stimulation blocks. Black dots represent individual STNs. Linear mixed-effects models (LME) reveal no significant modulation between blocks (see text). Initial frequency and initial amplitude refer to the value of the first 10-s bin. **C.** Amplitude characteristics of the ERNA at the group level and across stimulation blocks. Linear mixed-effects models reveal a significant modulation of the maximal amplitude ( $b = -0.06$ ,  $t_{(38)} = -3.56$ ,  $p = .013$ ) and the time to reach the steady state ( $b = -6.27$ ,  $t_{(38)} = -2.21$ ,  $p = .03$ ) over blocks. *Bottom right;* Averaged amplitude of the ERNA for block 1 and block 4 (mean  $\pm$  SEM). (For interpretation of the references to colour in this figure legend, the reader is referred to the web version of this article.)

( $4.9 \pm 0.4$  on average, see Methods for criteria) lasting for  $24 \pm 2$  ms on average after the cessation of the stimulation. The initial frequency of the ERNA, measured as the inverse of the delay between the first two peaks, was similar to the steady state of the ERNA during stimulation (initial frequency:  $271.3 \pm 11.7$  Hz and ERNA steady state:  $263.2 \pm 2.1$  Hz, paired  $t$ -test,  $t_{(10)} = 0.82$ ,  $p = .43$ ). Note that two STNs with an evoked potential during stimulation did not meet our criteria for an ERNA response at offset of stimulation, although both had an evoked response during stimulation (patients 2 and 7).

Moreover, this analysis confirmed the absence of an ERNA following cessation of stimulation in patients 12 to 14 (Table 2, Fig. S1).

In order to study the modulation of the ERNA by preceding stimulation we examined the data from 7 hemispheres (5 patients) in which a second experimental condition was performed. In this paradigm DBS was applied for a shorter period of time ( $14.1 \pm 2$  s). The comparison of the resonant activity after short versus long DBS blocks revealed a more marked ERNA after short stimulation blocks which lasted longer ( $29.4 \pm 2$  ms vs  $21.7 \pm 1$  ms, paired  $t$ -tests:  $t_{(6)} = 3.3$ ,  $p = .024$ ) with

## A Patient 5: ERNA in time domain



## B Group Data

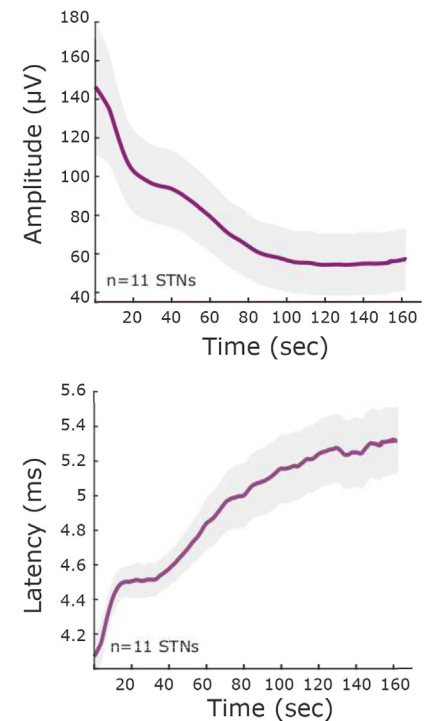


**Fig. 3.** ERNA during long stimulation blocks (condition 1) in the temporal domain. **A. Left:** LFP traces at the start, when largest amplitude is reached, the middle (after 60 s) and the end of the first long duration stimulation block of patient 5, revealing the presence of a changing evoked response between stimulation artefacts. **Right:** Superimposition of 260 pulses (grey) and their average (blue). To demonstrate the changing nature of the evoked activity over time we selected the maximal discrete peak between the stimulus artefacts in the first interval, tracked this peak throughout the stimulation block (indicated with a black arrowhead) and measured the amplitude and latency of this evoked potential. **B.** Change in the averaged amplitude and latency of the selected peak over time at the group level (mean  $\pm$  SEM). (For interpretation of the references to colour in this figure legend, the reader is referred to the web version of this article.)

more waves observed ( $7.3 \pm 0.6$  vs  $4.4 \pm 0.2$ , paired t-test:  $t_{(6)} = 4.06$ ,  $p = .007$ ). In addition, the initial frequency and amplitude of the ERNA were significantly higher after short stimulations ( $t_{(6)} = 5.2$ ,  $p = .002$  and  $t_{(6)} = 2.48$ ,  $p = .047$ , Fig. 4B). This change in ERNA character following short and long duration stimulation periods is in line with the shift to a lower steady state frequency during long duration stimulation evident in the ERNA in the spectral domain (Fig. 2A).

With the exception of patients 2 and 7, the ERNA following cessation of stimulation consisted of several waves lasting longer than the inter-stimulus interval (ISI) during DBS at 130 Hz. This raises the possibility that the steady state response during stimulation reflected the temporal summation of overlapping evoked responses, where each lasts longer than the ISI (see Fig. 4C).

### 3.3. Stimulation related dynamics in beta oscillations

The time–frequency plots showed a decrease in beta oscillatory activity during continuous stimulation at 130 Hz, and a delayed return of beta activity upon cessation of stimulation (labelled with “3” in Fig. 1C). The suppression during and the delayed return of beta activity are consistent with previous findings (Kühn et al., 2008; Eusebio et al., 2011; Quinn et al., 2015; Whitmer et al., 2012), but the precise time-course of beta suppression once stimulation has begun has not been previously quantified. For each stimulation block, time-evolving power changes were computed in the beta frequency band (13–34 Hz) in two 30-s windows aligned to the first or last stimulation artefact (Fig. 5A). To allow the comparison with the previous ERNA analysis, only the STNs showing an ERNA during stimulation were considered in the following analysis (Table 2, patients 1 to 11,  $n = 13$ ). However, due to

the contamination of the lower frequencies by involuntary movements unequal numbers of STNs were analysed in consecutive stimulation blocks (see Fig. 5A and Fig. 6C). The averaged time courses revealed a rapid and sustained suppression of beta power during DBS followed by a slower return to baseline level when DBS was switched off. The first significant reduction of beta power ( $p < .05$  after FDR correction) was observed within the first 500 ms of stimulation (including a 200 ms period in which stimulation amplitude was ramped up) in all the blocks, whereas the baseline level was on average reached  $8.9 \pm 2.7$  s after cessation of stimulation.

To quantify the dynamics of the stimulation-induced changes in the beta activity and compare them across consecutive blocks we averaged the beta percentage change in shorter epochs of 10 s within the two previously defined time windows (Fig. 5B). Linear mixed-effects modelling indicated that the initial beta suppression was similar across the four consecutive blocks ( $b = 1.9$ ,  $t_{(30)} = 1.1$ ,  $p = .31$ ). There was a trend for beta suppression to reduce after long and repeated stimulation but this did not reach significance ( $b = 2.9$ ,  $t_{(28)} = -2.1$ ,  $p = .054$ ). During the washout epoch, the linear mixed-effects modelling was not significant across blocks ( $b = -3.66$ ,  $t_{(27)} = -1.23$ ,  $p = .23$ ).

In the three STNs showing no ERNA, either during or after stimulation blocks (see Table 2 and Fig. S1), the averaged beta power was reduced during stimulation in two of them (subject 12: averaged beta reduction of  $20.1 \pm 5.5\%$  across the 3 blocks; subject 14:  $26.7 \pm 0.2\%$ ). In subject 13, there was no significant change in beta in the three stimulation blocks (averaged beta increase of  $5.6 \pm 4.7\%$  across the 3 blocks).

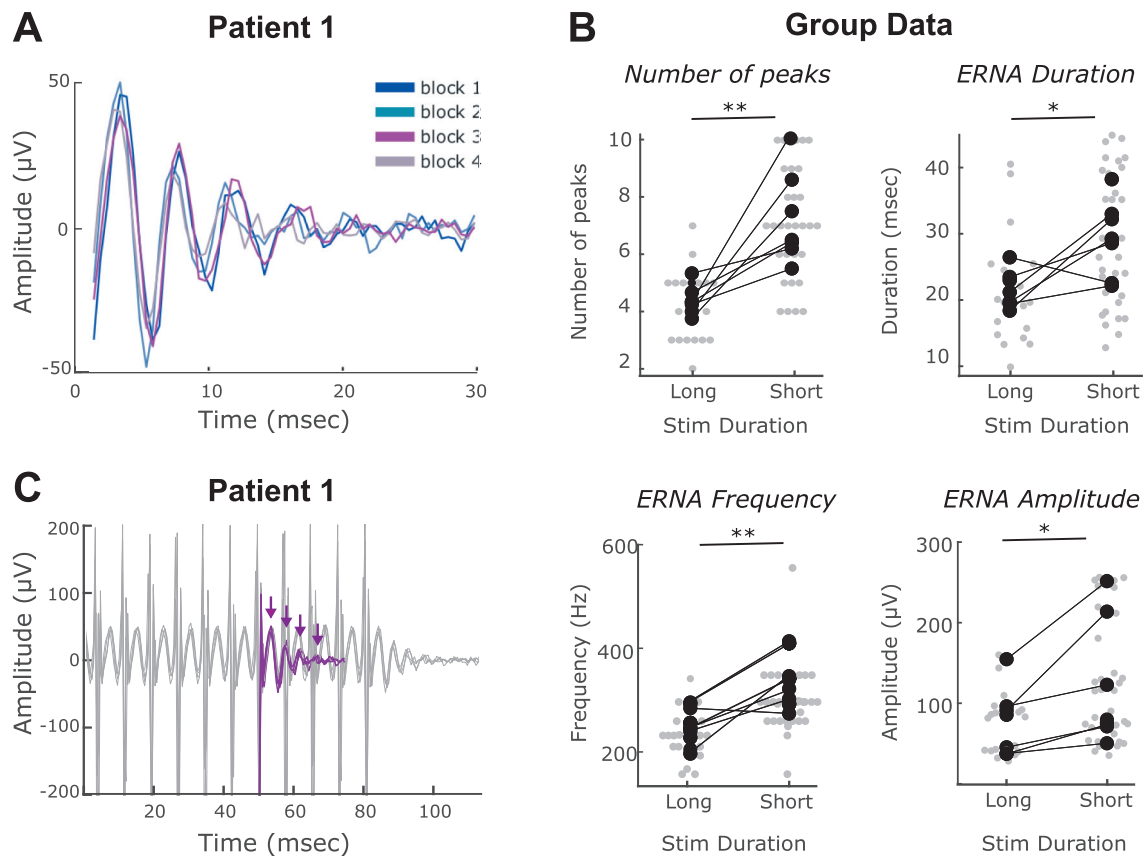


**Fig. 4.** ERNA after DBS. **A.** The ERNA is characterised by a series of high frequency waves following cessation of stimulation (time 0). These waves progressively diminish in amplitude and frequency. Note that the first 1.5 ms (starting from the peak of the stimulation artefact) have been cut to avoid any contamination by the stimulation artefact. The ERNA observed after the four long blocks of stimulation are superimposed. **B.** The ERNA is more marked after short than long stimulation blocks. Grey dots; all individual ERNA for all blocks and STN. Black dots: averaged values for each STN. Grey dots are the results of individual stimulation blocks. Paired *t*-tests, \*  $p < .05$ , \*\*  $p < .01$ . **C.** ERNA after DBS superimposed on the ERNA observed during DBS.

### 3.4. Non-frequency selectivity of DBS induced power suppression

The frequency selectivity of DBS power suppression was tested by quantifying the averaged power suppression across all blocks in three other frequency bands; alpha/theta (4–12 Hz), low gamma (35–45 Hz) and high gamma (70–90 Hz). Note that to avoid line noise, windows were selected excluding the 50 and 100 Hz bands. In addition to the beta power suppression ( $t_{(11)} = 4.75$ ,  $p < .001$ ), there was a significant decrease in low gamma power during stimulation ( $t_{(11)} = 3.86$ ,  $p = .003$ , Fig. 6A). Based on these results we decided to explore the temporal evolution of power changes in this frequency band with the same procedure as for the beta band. When signals were aligned to the start of the stimulation, we observed an abrupt reduction in low gamma power, starting after 125 to 375 ms across the four stimulation blocks and maintained throughout the entire stimulation (Fig. 6C). The averaged initial power suppression was similar between the four stimulation blocks ( $b = 2.8$ ,  $t_{(30)} = 1.1$ ,  $p = .27$ ), as was the averaged power suppression in the last 10 s of stimulation ( $b = 0.8$ ,  $t_{(28)} = 0.73$ ,  $p = .47$ , Fig. 6B). Thus, when DBS was switched on the low gamma power was rapidly suppressed, as previously observed for beta power. The two frequency bands however showed different patterns when DBS was switched off. As illustrated in Fig. 6D, after cessation of the stimulation, low gamma power returned faster to its baseline level, showing a slight overshoot ( $3.8 \pm 0.9$  s across all blocks and sides), than beta power ( $8.9 \pm 2.7$  s, Wilcoxon signed-rank test;  $Z = 33$ ,  $p = .039$ ).

### 3.5. Dynamics in high frequency oscillations (HFO)

The ERNA elicited by stimulation occurs in the same frequency range as HFO (200–400 Hz). As suggested by the time frequency plot of patient 5, the HFO activity seemed to decrease in frequency during DBS (Fig. 1C, label 4). To test the modulation of this high frequency activity we identified the HFO frequency peak in the absence of stimulation (to avoid contamination by the ERNA, see methods) in five 20-s time windows; one during the baseline, two immediately following long duration blocks of DBS, and two at the end of the resting periods between such blocks (Fig. 7A). Note that only the first two DBS blocks were considered to keep enough data points across all the tested STNs ( $n = 13$  STNs) as 2 patients performed only two long duration stimulation blocks. A clear HFO peak was found in the baseline period in six STNs (five patients), with a peak frequency of  $242.5 \pm 2.8$  Hz, significantly less than the initial ( $t_{(5)} = -30.8$ ,  $p < .001$ ) or steady state frequency of the ERNA ( $t_{(5)} = -5.26$ ,  $p = .033$ ). The peak frequencies of these HFO were significantly modulated across the five different time windows ( $b = -5.1$ ,  $t_{(26)} = -2.82$ ,  $p = .01$  Fig. 7B). After the first stimulation block, the HFO frequency was found to be significantly decreased compared to baseline (OFF1:  $t_{(5)} = 4.85$ ,  $p = .005$ ), before increasing again and reaching a frequency close to baseline in the last 20 s of the resting period without stimulation ( $t_{(5)} = 1.8$ ,  $p = .13$ ). This pattern was also observed after the second stimulation block with an initial reduction of the HFO frequency compared to the baseline ( $t_{(5)} = 4.089$ ,  $p = .008$ ) or the end of the previous rest period ( $t_{(5)} = 3.67$ ,  $p = .02$ ). Again, over the following rest period the HFO peaks increased in frequency ( $t_{(5)} = -5.6$ ,  $p = .005$ ) without, however, reaching the frequency observed during the baseline ( $t_{(5)} = 3.44$ ,

## A Time courses of beta power

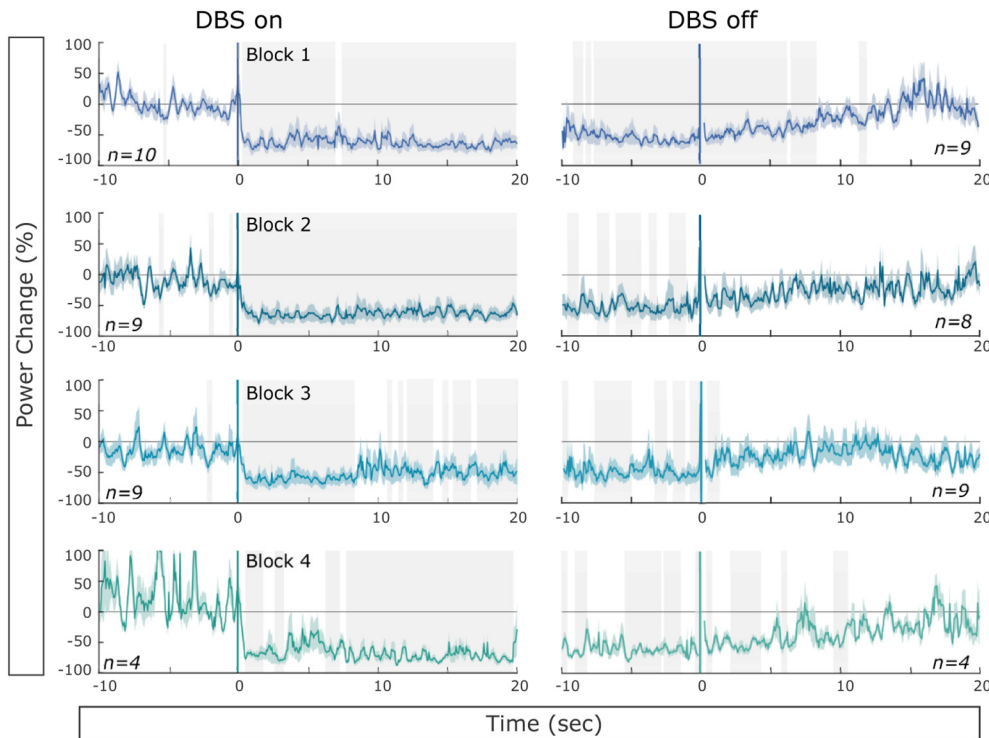
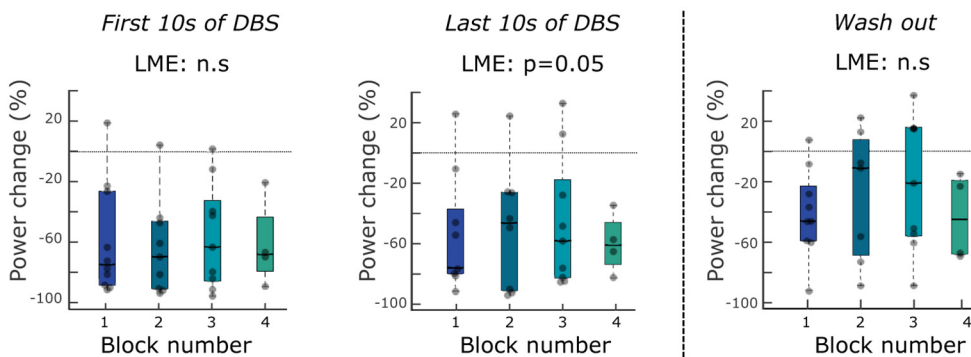


**Fig. 5.** Modulation of beta power induced by DBS. A. Averaged time course of % beta power change relative to baseline (rest, without stimulation) aligned to the first (left) and last (right) stimulation artefact for four consecutive stimulation blocks. Mean  $\pm$  SEM of %change from baseline power is shown. Note that, because we skipped data where movement occurred, the number of STN (given by n) included differs between windows. The periods during which the beta power was significantly different to zero are indicated by the grey shading (one sample t-test,  $p < .05$  after FDR correction). B. Comparison of averaged beta power changes in the first and last 10s of DBS between the four consecutive blocks. Linear mixed-effects models (LME) revealed a trend for the last 10s of DBS to differ ( $b = 2.9$ ,  $t_{(28)} = -2.1$ ,  $p = .054$ ).

## B Beta changes in 10sec epochs



$p = .026$ ). Note that some authors describe two HFO peaks (Özkurt et al., 2011), one centred around 250 Hz and another at higher frequencies, with the latter peak preferentially occurring after treatment with levodopa. We did not detect a peak at higher frequencies when not stimulating, as our patients were recorded off medication.

### 3.6. Clinical correlations

As previously reported (Neumann et al., 2016), we confirmed the correlation between normalised baseline beta power and the contralateral UPDRS motor hemibody score OFF medication assessed pre-operatively ( $r = 0.67$ ,  $p = .024$ ; see Fig. 8). In addition, there was a trend towards a significant correlation between baseline beta power and the UPDRS difference between OFF-ON medication ( $r = 0.58$ ,  $p = .06$ ). In a further exploratory analysis we correlated the different ERNA parameters with the pre-operative contralateral motor UPDRS scores. This revealed a significant positive correlation between the time taken for the ERNA amplitude to reach steady state and both the UPDRS score OFF medication ( $r = 0.58$ ,  $p = .037$ ) and the difference between

UPDRS OFF and ON ( $r = 0.62$ ,  $p = .024$ ; see Fig. 8). For both the beta power and the ERNA parameters, no significant correlation was observed with the ipsilateral motor UPDRS scores.

## 4. Discussion

Here we analyse and contrast the evoked and induced changes in STN activity in response to DBS of this target. The evoked response or ERNA recorded during high frequency stimulation is known to initially increase in amplitude at the start and then to decrease in both frequency and amplitude over the course of a 60–90 s block of stimulation (Sinclair et al., 2019b). Here we describe these dynamics in greater detail, demonstrating that steady state frequency and amplitude are reached after a minute or so of stimulation, and show a previously unreported further diminution of maximal ERNA amplitude when long duration blocks of stimulation are repeated. When stimulation ceases, or more generally when stimulation frequency is low enough, the ERNA is exposed as a series of waves of diminishing amplitude (Sinclair et al., 2019b, 2018). Here we show that these waves last longer after cessation

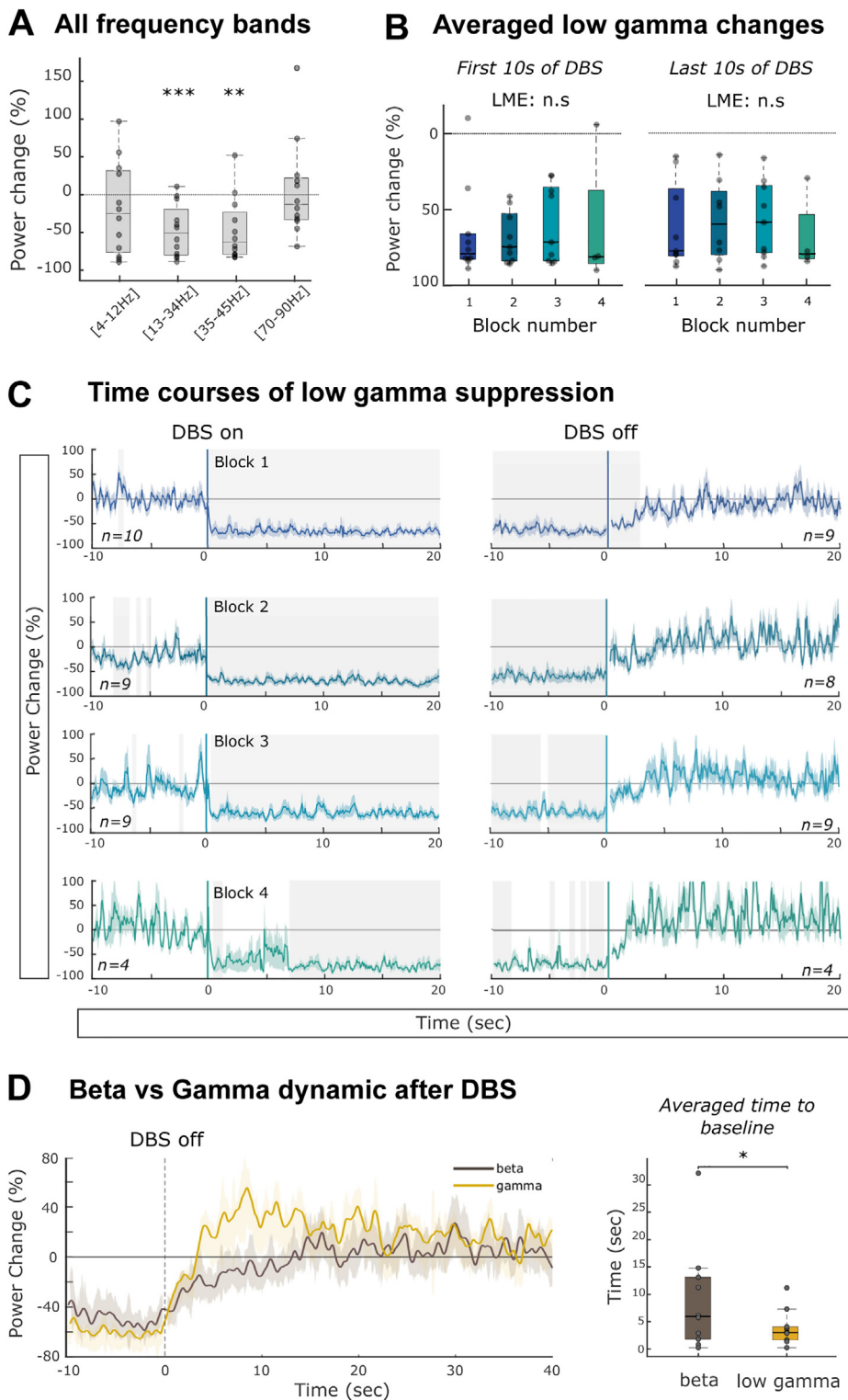


**Fig. 6.** DBS modulation of LFP in other frequency bands. **A.** Averaged power changes in the four frequency bands. One sample t-test, \*\*  $p < .01$ , \*\*\*  $p < .001$ . **B.** Averaged low gamma power changes in the first and last 10s of DBS. Both are similar across the four stimulation blocks (linear mixed-effects models, LME,  $b = 3.0$ ,  $t_{(33)} = 1.3$ ,  $p = .21$  and  $b = 0.2$ ,  $t_{(23)} = 0.14$ ,  $p = .89$ ). **C.** Averaged time course of low gamma power aligned to the first (left) and last (right) stimulation artefact for four consecutive stimulation blocks. Note that, because we skipped data where movement occurred, the number of STNs (given by  $n$ ) included differs between windows. The periods during which the low gamma power was significantly different to zero are indicated by grey shading (one sample t-test,  $p < .05$  after FDR correction). **D.** Comparison of power recurrence after cessation of DBS. *Left:* averaged group dynamics of spectral signals. *Right:* Power recurrence to baseline across spectral components. Wilcoxon signed rank test, \*  $p < .05$ .

of short periods of stimulation than after longer periods of stimulation. In contrast, DBS rapidly suppresses beta and low gamma band activity in the STN LFP and steady state levels are thereafter relatively maintained during stimulation. In addition, the frequency of HFO in the STN is below that of the ERNA, and is further reduced during DBS.

#### 4.1. Origin of the ERNA

The ERNA consists of high amplitude and brief waves of local

activity time-locked to and evoked by stimulation pulses. One possibility raised by the evoked nature of the ERNA is that it is due to axonal stimulation of inputs to the STN and is an analogue of the fibre volleys measured *in vitro*, or compound action potentials measured *in vivo*, or, related to this, it represents the post-synaptic response to synchronised fibre volleys. Compound action potentials in the STN due to orthodromic axonal stimulation of afferents have onset latencies of a millisecond or so (Gmel et al., 2015), and would have been obscured by the stimulation artefact and relatively low sampling rate in our study.

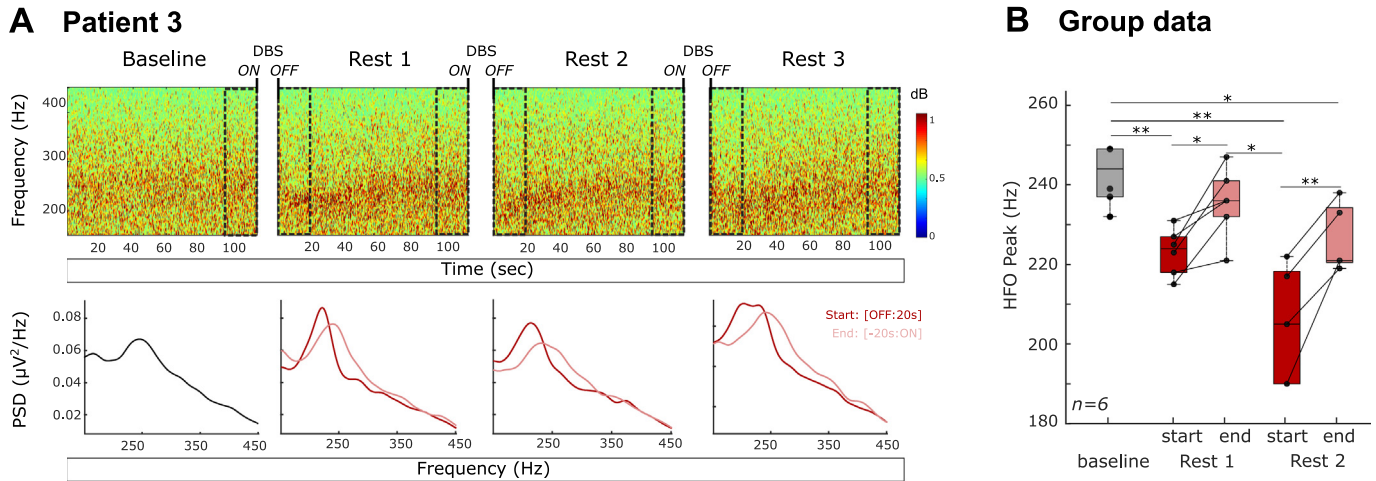
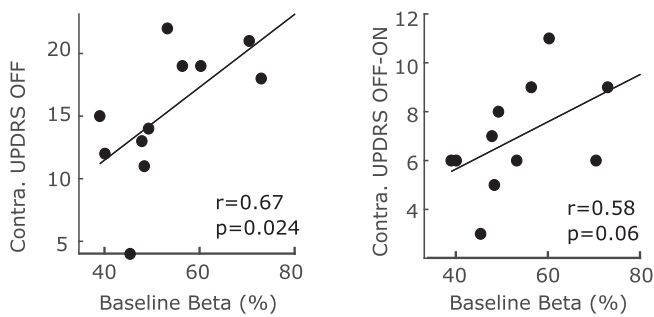


**Fig. 7.** Modulation of HFO by DBS. A. Time frequency plots of the baseline and the 3 resting periods between long duration stimulation blocks in the HFO frequency range for one patient. Power spectral densities were computed in 20 s windows as indicated by the dashed rectangles and either followed cessation of stimulation (OFF: 20s) or preceded stimulation (-20s: ON). B. HFO peaks are significantly different between the baseline and the two first resting periods ( $b = -5.1$ ,  $t_{(26)} = -2.82$ ,  $p = .01$ ). Following paired t-test with FDR correction, \*,  $p < .05$ , \*\*  $p < .01$ .

### A Baseline Beta Power



### B ERNA time to reach steady state

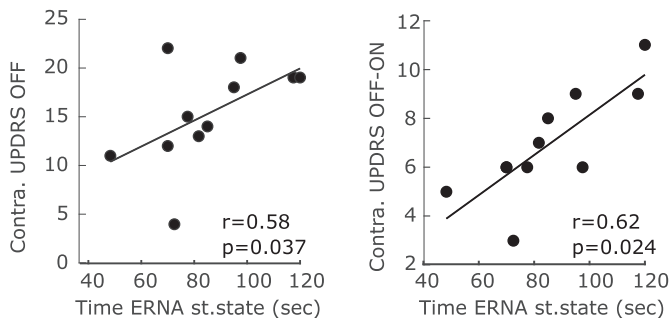


**Fig. 8.** Clinical correlations. A. Correlation between normalised baseline beta power and both the contralateral UPDRS Part III motor hemibody score OFF and the difference between OFF and ON medication state. Spearman correlation. Black dots; individual STN. B. Similar correlation with the time to reach the ERNA steady state amplitude. Diff: difference between UPDRS OFF and ON medication state.

However, longer latency compound action potentials may also be recorded in the STN and may reflect recurrent discharge due to antidromic stimulation of the cerebral cortex through the hyperdirect pathway (Gmel et al., 2015; Johnson et al., 2020; Miocinovic et al., 2018; Walker et al., 2012), or possibly of recurrent discharge due to stimulation of more local targets like the globus pallidus (Ramirez-Zamora et al., 2020). In support of an origin of the ERNA related to

synchronised fibre volleys or the subsequent post-synaptic response to them, both are reported to diminish in amplitude and increase in latency during prolonged high frequency stimulation, due to the effects of progressive axonal and synaptic failure (Rosenbaum et al., 2014; Steiner et al., 2019). Short-term synaptic depression during high frequency stimulation is mediated by decreased presynaptic calcium influx, desensitisation and saturation of postsynaptic receptors and fewer release-competent vesicles (Schneggenburger et al., 2002). While the readily releasable vesicle pool and recycling pool in the presynapse are exhausted within milliseconds to seconds, the reserve vesicle pool is released during unphysiological high-frequency stimulation with slower release kinetics and can last for tens of seconds to minutes. One possibility therefore is that the initial increase in ERNA amplitude relates to the short-lived increase in synaptic release or post-synaptic potentiation during high frequency stimulation, and the progressive relative exhaustion of the reserve vesicle pool thereafter accounts for the drift to steady-state of the ERNA at lower amplitude and frequency (Denker and Rizzoli, 2010; Rizzoli and Betz, 2005). This hypothesis is supported by the observation that the progressive diminution of ERNA frequency and amplitude is absent when stimulation is applied at only 20 Hz (Sinclair et al., 2019b), as diminution of the reserve vesicle pool only occurs with high frequency stimulation (Rizzoli and Betz, 2005).

The above, however, does not explain the repetitive nature of the ERNA unless it is assumed that the response to stimulation of the hyperdirect or indirect pathways is repetitive. Another possible mechanism for the ERNA is that it reflects an exaggeration of the network responsible for spontaneously occurring HFO at rest (Sinclair et al., 2019b). However, the HFO in our series had a lower initial frequency than the ERNA, was driven to an even lower frequency, distinct from that of the ERNA, during long duration stimulation and was only present in less than half of cases demonstrating the ERNA. In contrast, though, Sinclair et al. (2019b) reported that the median HFO peak frequency immediately post-DBS shared the same frequency as the ERNA during clinical stimulation.

#### 4.2. Dynamics of the ERNA during and after DBS

A particular focus of the current study were the frequency and amplitude dynamics of the ERNA. The cessation of stimulation reveals that the ERNA consists of a series of oscillations at a similar frequency to the steady state oscillation during stimulation, but of diminishing amplitude. Such ‘ringing’ is suggestive of an underdamped resonance, although it is possible that each wave is an independent evoked

component. During continued stimulation, after a brief amplitude increase, there is a progressive drop in both the ERNA frequency and amplitude until a steady state is reached. Assuming resonance, the drop in frequency and amplitude would be consistent with the increasing damping of a driven oscillation that reaches and holds peak damping during the steady state recording. These two damping processes seen during and at the end of stimulation may be one-and-the-same. Thus, if stimulation is ended early, before steady state amplitude and frequency are reached, then the cessation of stimulation is followed by a ringing with a higher initial amplitude and greater number of wave cycles, consistent with reduced damping.

Two subjects did not show ringing upon termination of stimulation, although, like others, they demonstrated an evoked activity during stimulation. In these two cases we suggest that the damping process was more marked leading to critical damping of the oscillations so that these were not seen as repetitive on cessation of stimulation. More importantly, with respect to some of the potential clinical applications to be discussed later, these two cases raise the possibility that a multiphasic ERNA may not be consistently seen during chronic DBS.

Although a damped resonance might describe the neural network behaviour it does not define the underlying mechanisms. We suggest that damping might be due to the effects of relative axonal failure and synaptic depression discussed above (Rosenbaum et al., 2014; Steiner et al., 2019). Even so the nature of the resonance that is damped is unclear. The correlation between the time for the ERNA to reach steady-state and the severity of contralateral motor impairment off medication might suggest that resonance is stronger when the Parkinsonian state is worse. The correlation between the time for the ERNA to reach steady state and the degree of improvement possible with levodopa might further suggest that resonance is exaggerated by dopaminergic under activity. A key question is whether the time taken to establish damping of the evoked response may be related to the time taken for the development of clinical DBS effects. This would necessitate frequent probing of motor function over the first minute or two after stimulation onset; data that is not available in the literature.

#### 4.3. Dynamics of background activities in response to DBS

Beta band oscillations in the STN LFP occur spontaneously, without the need for extrinsic stimulation (Brown et al., 2001). Their amplitude is one to two orders of magnitude less than that of the ERNA suggesting that, although post-synaptic in origin, they represent either a far less tightly synchronised activity in time, a sparser synchronisation in space, or both. This synchronisation is coupled to cortical activity at the same frequency, but lags this by about 20 ms, and is diminished by voluntary movement (Oswal et al., 2013). Beta amplitude in the STN correlates with pre-operative assessments of motor impairment (Neumann et al., 2016), as confirmed here. Gamma band oscillations in the STN LFP are also recorded at rest, but are of even smaller amplitude, tending to be increased as a broad band activity during voluntary movement. This increase during movement has led to speculation that they are somehow involved in the coding of movement (Oswal et al., 2013).

The dynamics of the response to the continuous 130 Hz stimulation of the STN differed between the ERNA and beta-low gamma activity. The ERNA, or its damping, evolved slowly as stimulation was maintained or repeated, whereas beta and gamma oscillations responded rapidly. These contrasting dynamics argue for differences in underlying mechanisms, with the rapid suppression and recovery of the beta and low gamma activity suggesting that this might be due to the more direct desynchronising effects of high-frequency stimulation. These may reflect chaotic desynchronisation (Wilson et al., 2011), or the driving of afferents to STN at high frequency, which supplants or over-rides pathological inputs at lower frequency (Birdno and Grill, 2008; Hashimoto et al., 2003; Moran et al., 2011). Both are physical phenomena that may be able to establish themselves and desynchronise population activity over relatively few stimulation cycles. The recovery

of beta activity following cessation of stimulation was, however, slower, as previously reported (Bronte-Stewart et al., 2009; Kühn et al., 2008), and might reflect the time taken for synchronisation to be re-established at the network level. The time course of beta recovery was similar to that reported for the acute return of bradykinesia and rigidity (Bronte-Stewart et al., 2009; Kühn et al., 2009; Levin et al., 2009), but there are additional slower recovery dynamics likely in rigidity, tremor, axial impairment and postural instability (Koop et al., 2006; Shivitz et al., 2006; Temperli et al., 2003; Vaillancourt et al., 2006). Whether the decrement in maximal ERNA amplitude following repeated long duration blocks of high frequency stimulation relates to some of these slower symptom modulations seen with DBS requires further investigation.

#### 4.4. Implications and applications of evoked and induced responses to DBS

The differing dynamics between the ERNA and beta activity have implications with regard to their use as feedback signals in adaptive DBS. Specifically, the rapid response of beta activity to the onset and offset of stimulation means that it can be used to target beta bursts in the STN (Little et al., 2013, 2016b, 2016a; Tinkhauser et al., 2017a; Velisar et al., 2019). These are increasingly reported to play a key role in the mechanism of bradykinesia and rigidity in PD (Deffains et al., 2018; Tinkhauser et al., 2020, 2017a, 2017b; Torrecillos et al., 2018). The ERNA does not provide direct feedback relevant to beta bursts and undergoes relatively slow changes with respect to the duration of stimulation. The ERNA could potentially better subserve more slowly responsive control algorithms (Arlotti et al., 2018; Rosa et al., 2017). Both the ERNA and beta activity may be of additional value in localising the dorsal 'motor' region of the STN during surgery (Sinclair et al., 2018; Thevathasan et al., 2020; Zaidel et al., 2009), although it is possible that the former may be particularly well suited to this as, in one case it remained despite general anaesthesia (Sinclair et al., 2018). In addition, both activities may facilitate prediction of the optimal contact for stimulation following surgery (Chen et al., 2006b; Ince et al., 2010; Sinclair et al., 2018; Thevathasan et al., 2020; Tinkhauser et al., 2018; Yoshida et al., 2010).

The suppression of low gamma activity by DBS is interesting as this activity is thought to help encode voluntary movements. Accordingly its suppression by DBS may point to the non-specificity of this intervention and help explain some of the motoric deterioration that may complicate DBS. This is most clearly seen in isolated cranial dystonia patients, when high frequency stimulation of the pallidum can cause paradoxical motor deficits (Berman et al., 2009; Blahak et al., 2011; Huebl et al., 2015; Wolf et al., 2016). However, stimulation of the STN may also cause motor deficits. For example, this may be the case in verbal fluency, which is impaired by DBS (Parsons et al., 2006), and has been specifically linked to increased subthalamic gamma activity (Anzak et al., 2011). It may also help explain the modest impairments in limb motor function in PD patients who otherwise perform well when not stimulated, i.e. those subjects who have relatively good background motor performance at the time of testing (Chen et al., 2006a). The latter may also contribute to the impairment of swimming ability during STN DBS that has been recently highlighted (Waldvogel et al., 2020). Finally, the possibility should be acknowledged that the DBS induced suppression of LFP activity spread to even higher frequency bands than the low gamma range, but was masked by a coincidental rise in the noise floor of the amplifier during stimulation.

These considerations are important as they argue that patients may potentially never be able to achieve their optimal performance during conventional continuous DBS, which might be relatively indiscriminate in its effects on spontaneous oscillatory activity, and affect both pathological and physiological oscillations. Such observations help motivate the development of adaptive DBS approaches which partially spare residual physiological processing in the subthalamic nucleus by reducing the duration or intensity of stimulation (Arlotti et al., 2018; Little

et al., 2013), or by delivering phase-dependent stimulation according to neural feedback (Cagnan et al., 2017; Holt et al., 2019).

#### 4.5. Limitations of the study

Our results may have been confounded by the post-operative stun effect, which is known to lower beta activity (Chen et al., 2006b). In addition, we did not simultaneously evaluate clinical state during our recordings, which would be necessary to directly relate the dynamics of ERNA characteristics and of beta suppression to the dynamics of the clinical effects of DBS. This again would require a bigger cohort or the opportunity to record in chronically implanted patients to avoid confounding DBS related LFP changes with movement-related effects imposed by clinical testing. Moreover, the symmetric biphasic pulse used in the present study is not standard in clinical practice and our sampling rate of 2048 Hz might have been too low to precisely describe and follow the dynamics of the ERNA in the time domain. Finally, only 14 patients participated in our study and some of our contrasts involved small subsets of patients (see Fig. 5A and Fig. 6C), so that these results need to be confirmed in a larger series.

#### 5. Conclusions

We have characterised the temporal dynamics of different responses to DBS in the STN LFP, and speculated on the phenomena that may underlie these changes. In particular, the relatively slow development of damping evident in the ERNA after stimulation onset raises the possibility of an underlying progressive axonal and synaptic failure. Conversely, the very rapid onset of beta suppression following DBS onset may reflect more direct desynchronising effects of high-frequency stimulation. Notwithstanding the underlying mechanisms, the different temporal dynamics exhibited by evoked and induced activities in response to stimulation may impact on their use as feedback signals in adaptive DBS.

##### Credit author statement

Christoph Wiest: Investigation, Formal analysis, Writing – Review & Editing, Visualization.

Gerd Tinkhauser: Conceptualization, Funding acquisition, Investigation, Writing – Review & Editing.

Alek Pogosyan: Software.

Manuel Bange: Investigation, Writing – Review & Editing.

Muthuraman Muthuraman: Funding acquisition, Resources, Writing – Review & Editing.

Sergiu Groppa: Funding acquisition, Resources.

Fahd Baig: Investigation.

Abteem Mostofi: Investigation.

Erlick A. Pereira: Resources.

Huiling Tan: Writing – Review & Editing.

Peter Brown: Funding acquisition, Project administration, Conceptualization, Resources, Writing – Original Draft, Supervision.

Flavie Torrecillos: Conceptualization, Investigation, Formal analysis, Validation, Writing – Original Draft, Visualization, Supervision, Project administration.

#### Declaration of Competing Interest

None.

#### Acknowledgements

This work was supported by the Medical Research Council [MC\_UU\_12024/1], the National Institute for Health Research (NIHR) Oxford Biomedical Research Centre (BRC) and Rosetrees Trust. G.T. received project funding from the Swiss Parkinson Association. This work was further supported by a grant from the German Research

Council for S.G. and M.M. (CRC-TR-128). The neuroBi stimulator used in this study was provided by the Bionics Institute of Australia.

#### Appendix A. Supplementary data

Supplementary data to this article can be found online at <https://doi.org/10.1016/j.nbd.2020.105019>.

#### References

- Anzak, A., Gaynor, L., Beigi, M., Limousin, P., Hariz, M., Zrinzo, L., Foltynie, T., Brown, P., Jahanshahi, M., 2011. A gamma band specific role of the subthalamic nucleus in switching during verbal fluency tasks in Parkinson's disease. *Exp. Neurol.* 232, 136–142. <https://doi.org/10.1016/j.expneurol.2011.07.010>.
- Arlotti, M., Marceglia, S., Foffani, G., Volkmann, J., Lozano, A.M., Moro, E., Cogiamanian, F., Prenassi, M., Bocci, T., Cortese, F., Rampini, P., Barbieri, S., Priori, A., 2018. Eight-hours adaptive deep brain stimulation in patients with Parkinson disease. *Neurology* 90, e971–e976. <https://doi.org/10.1212/WNL.0000000000005121>.
- Benjamini, Y., Hochberg, Y., 1995. Controlling the false discovery rate: a practical and powerful approach to multiple testing. *J. R. Stat. Soc. Ser. B* 57, 289–300.
- Berman, B.D., Starr, P.A., Marks, W.J.J., Ostrem, J.L., 2009. Induction of bradykinesia with pallidal deep brain stimulation in patients with cranial-cervical dystonia. *Stereotact. Funct. Neurosurg.* 87, 37–44. <https://doi.org/10.1159/000195718>.
- Birdno, M.J., Grill, W.M., 2008. Mechanisms of deep brain stimulation in movement disorders as revealed by changes in stimulus frequency. *Neurother. J. Am. Soc. Exp. Neurother.* 5, 14–25. <https://doi.org/10.1016/j.nurt.2007.10.067>.
- Blahak, C., Capelle, H.-H., Baezner, H., Kinfe, T.M., Hennerici, M.G., Krauss, J.K., 2011. Micrographia induced by pallidal DBS for segmental dystonia: a subtle sign of hypokinesia? *J. Neural Transm.* 118, 549–553. <https://doi.org/10.1007/s00702-010-0544-y>.
- Bouthour, W., Mégevand, P., Donoghue, J., Lüscher, C., Birbaumer, N., Krack, P., 2019. Biomarkers for closed-loop deep brain stimulation in Parkinson disease and beyond. *Nat. Rev. Neurol.* 15, 343–352. <https://doi.org/10.1038/s41582-019-0166-4>.
- Bronte-Stewart, H., Barberini, C., Koop, M.M., Hill, B.C., Henderson, J.M., Wingeier, B., 2009. The STN beta-band profile in Parkinson's disease is stationary and shows prolonged attenuation after deep brain stimulation. *Exp. Neurol.* 215, 20–28. <https://doi.org/10.1016/j.expneurol.2008.09.008>.
- Brown, P., 2003. Oscillatory nature of human basal ganglia activity: relationship to the pathophysiology of Parkinson's disease. *Mov. Disord.* 18, 357–363. <https://doi.org/10.1002/mds.10358>.
- Brown, P., Oliviero, A., Mazzone, P., Insola, A., Tonali, P., Di Lazzaro, V., 2001. Dopamine Dependency of Oscillations between Subthalamic Nucleus and Pallidum in Parkinson's Disease. 21. pp. 1033–1038.
- Cagnan, H., Pedrosa, D., Little, S., Pogosyan, A., Cheeran, B., Aziz, T., Green, A., Fitzgerald, J., Foltynie, T., Limousin, P., Zrinzo, L., Hariz, M., Friston, K.J., Denison, T., Brown, P., 2017. Stimulating at the right time: phase-specific deep brain stimulation. *Brain* 140, 132–145. <https://doi.org/10.1093/brain/aww286>.
- Chen, C.C., Brücke, C., Kempf, F., Kupsch, A., Lu, C.S., Lee, S.T., Tisch, S., Limousin, P., Hariz, M., Brown, P., 2006a. Deep brain stimulation of the subthalamic nucleus: a two-edged sword. *Curr. Biol.* <https://doi.org/10.1016/j.cub.2006.10.013>.
- Chen, C.C., Pogosyan, A., Zrinzo, L.U., Tisch, S., Limousin, P., Ashkan, K., Yousry, T., Hariz, M.I., Brown, P., 2006b. Intra-operative recordings of local field potentials can help localize the subthalamic nucleus in Parkinson's disease surgery. *Exp. Neurol.* 198, 214–221. <https://doi.org/10.1016/j.expneurol.2005.11.019>.
- Deffains, M., Iskhakova, L., Katabi, S., Israel, Z., Bergman, H., 2018. Longer  $\beta$  oscillatory episodes reliably identify pathological subthalamic activity in parkinsonism. *Mov. Disord.* 33, 1609–1618. <https://doi.org/10.1002/mds.27418>.
- Denker, A., Rizzoli, S.O., 2010. Synaptic vesicle pools: an update. *Front. Synaptic Neurosci.* 2, 1–12. <https://doi.org/10.3389/fnsyn.2010.00135>.
- Eusebio, A., Thevathasan, W., Doyle Gaynor, L., Pogosyan, A., Bye, E., Foltynie, T., Zrinzo, L., Ashkan, K., Aziz, T., Brown, P., 2011. Deep brain stimulation can suppress pathological synchronisation in parkinsonian patients. *J. Neurol. Neurosurg. Psychiatry* 82, 569–573. <https://doi.org/10.1136/jnnp.2010.217489>.
- Gmel, G.E., Hamilton, T.J., Obradovic, M., Gorman, R.B., Single, P.S., Chenery, H.J., Coyne, T., Silburn, P.A., Parker, J.L., 2015. A new biomarker for subthalamic deep brain stimulation for patients with advanced Parkinson's disease—a pilot study. *J. Neural Eng.* 12, 66013. <https://doi.org/10.1088/1741-2560/12/6/066013>.
- Hashimoto, T., Elder, C.M., Okun, M.S., Patrick, S.K., Vitek, J.L., 2003. Stimulation of the subthalamic nucleus changes the firing pattern of pallidal neurons. *J. Neurosci.* 23, 1916–1923. <https://doi.org/10.1523/JNEUROSCI.23-05-01916.2003>.
- Holt, A.B., Kormann, E., Gulberti, A., Pötter-Nerger, M., McNamara, C.G., Cagnan, H., Baaske, M.K., Little, S., Köppen, J.A., Buhmann, C., Westphal, M., Gerloff, C., Engel, A.K., Brown, P., Hamel, W., Moll, C.K.E., Sharott, A., 2019. Phase-dependent suppression of Beta oscillations in Parkinson's disease patients. *J. Neurosci.* 39, 1119–1134. <https://doi.org/10.1523/JNEUROSCI.1913-18.2018>.
- Horn, A., Li, N., Dembek, T.A., Kappel, A., Boulay, C., Ewert, S., Tietze, A., Husch, A., Perera, T., Neumann, W.-J., Reiser, M., Si, H., Oostenveld, R., Rorden, C., Yeh, F.-C., Fang, Q., Herrington, T.M., Vorwerk, J., Kühn, A.A., 2019. Lead-DBS v2: towards a comprehensive pipeline for deep brain stimulation imaging. *Neuroimage* 184, 293–316. <https://doi.org/10.1016/j.neuroimage.2018.08.068>.
- Huebl, J., Brücke, C., Schneider, G.-H., Blahak, C., Krauss, J.K., Kühn, A.A., 2015. Bradykinesia induced by frequency-specific pallidal stimulation in patients with cervical and segmental dystonia. *Parkinsonism Relat. Disord.* 21, 800–803. <https://doi.org/10.1016/j.parkreldis.2015.07.010>.

- [doi.org/10.1016/j.parkreldis.2015.04.023](https://doi.org/10.1016/j.parkreldis.2015.04.023).
- Ince, N.F., Gupta, A., Wichmann, T., Ashe, J., Henry, T., Bebler, M., Eberly, L., Aboosh, A., 2010. Selection of optimal programming contacts based on local field potential recordings from subthalamic nucleus in patients with Parkinson's disease. *Neurosurgery* 67, 390–397. <https://doi.org/10.1227/01.NEU.0000372091.64824.63>.
- Johnson, L.A., Wang, J., Nebeck, S.D., Zhang, J., Johnson, M.D., Vitek, J.L., 2020. Direct activation of primary motor cortex during subthalamic but not pallidal deep brain stimulation. *J. Neurosci.* 40, 2480–2519. <https://doi.org/10.1523/jneurosci.2480-19.2020>.
- Koop, M.M., Andrzejewski, A., Hill, B.C., Heit, G., Bronte-Stewart, H.M., 2006. Improvement in a quantitative measure of bradykinesia after microelectrode recording in patients with Parkinson's disease during deep brain stimulation surgery. *Mov. Disord.* 21, 673–678. <https://doi.org/10.1002/mds.20796>.
- Kühn, A.A., Kupsch, A., Schneider, G.-H., Brown, P., 2006. Reduction in subthalamic 8-35 Hz oscillatory activity correlates with clinical improvement in Parkinson's disease. *Eur. J. Neurosci.* 23, 1956–1960. <https://doi.org/10.1111/j.1460-9568.2006.04717.x>.
- Kühn, A.A., Kempf, F., Brücke, C., Gaynor Doyle, L., Martinez-Torres, I., Pogoyan, A., Trottenberg, T., Kupsch, A., Schneider, G.-H., Hariz, M.I., Vandenbergh, W., Nuttin, B., Brown, P., 2008. High-frequency stimulation of the subthalamic nucleus suppresses oscillatory beta activity in patients with Parkinson's disease in parallel with improvement in motor performance. *J. Neurosci.* 28, 6165–6173. <https://doi.org/10.1523/JNEUROSCI.0282-08.2008>.
- Kühn, A.A., Tsui, A., Aziz, T., Ray, N., Brücke, C., Kupsch, A., Schneider, G.-H., Brown, P., 2009. Pathological synchronization in the subthalamic nucleus of patients with Parkinson's disease relates to both bradykinesia and rigidity. *Exp. Neurol.* 215, 380–387. <https://doi.org/10.1016/j.expneurol.2008.11.008>.
- Levin, J., Krafczyk, S., Valkovic, P., Eggert, T., Claassen, J., Bötzel, K., 2009. Objective measurement of muscle rigidity in Parkinsonian patients treated with subthalamic stimulation. *Mov. Disord.* 24, 57–63. <https://doi.org/10.1002/mds.22291>.
- Little, S., Brown, P., 2020. Debugging adaptive deep brain stimulation for Parkinson's disease. *Mov. Disord.* 35, 555–561. <https://doi.org/10.1002/mds.27996>.
- Little, S., Pogoyan, A., Neal, S., Zavala, B., Zrinzo, L., Hariz, M., Foltynie, T., Limousin, P., Ashkan, K., FitzGerald, J., Green, A.L., Aziz, T.Z., Brown, P., 2013. Adaptive deep brain stimulation in advanced Parkinson disease. *Ann. Neurol.* 74, 449–457. <https://doi.org/10.1002/ana.23951>.
- Little, S., Beudel, M., Zrinzo, L., Foltynie, T., Limousin, P., Hariz, M., Neal, S., Cheeran, B., Cagnan, H., Gratwicke, J., Aziz, T.Z., Pogoyan, A., Brown, P., 2016a. Bilateral adaptive deep brain stimulation is effective in Parkinson's disease. *J. Neurol. Neurosurg. Psychiatry* 87, 717–721. <https://doi.org/10.1136/jnnp-2015-310972>.
- Little, S., Tripoliti, E., Beudel, M., Pogoyan, A., Cagnan, H., Herz, D., Bestmann, S., Aziz, T., Cheeran, B., Zrinzo, L., Hariz, M., Hyam, J., Limousin, P., Foltynie, T., Brown, P., 2016b. Adaptive deep brain stimulation for Parkinson's disease demonstrates reduced speech side effects compared to conventional stimulation in the acute setting. *J. Neurol. Neurosurg. Psychiatry*. <https://doi.org/10.1136/jnnp-2016-313518>.
- Lopiano, L., Torre, E., Benedetti, F., Bergamasco, B., Perozzo, P., Pollo, A., Rizzone, M., Tavezza, A., Lanotte, M., 2003. Temporal changes in movement time during the switch of the stimulators in Parkinson's disease patients treated by subthalamic nucleus stimulation. *Eur. Neurol.* 50 (2), 94–99. <https://doi.org/10.1159/000072506>.
- Lozano, A.M., Lipsman, N., Bergman, H., Brown, P., Chabardes, S., Chang, J.W., Mathews, K., McIntyre, C.C., Schlaepfer, T.E., Schulder, M., Temel, Y., Volkman, J., Krauss, J.K., 2019. Deep brain stimulation: current challenges and future directions. *Nat. Rev. Neurol.* 15, 148–160. <https://doi.org/10.1038/s41582-018-0128-2>.
- Miocinovic, S., de Hemptinne, C., Chen, W., Isbaine, F., Willie, J.T., Ostrem, J.L., Starr, P.A., 2018. Cortical potentials evoked by subthalamic stimulation demonstrate a short latency Hyperdirect pathway in humans. *J. Neurosci.* 38, 9129–9141. <https://doi.org/10.1523/JNEUROSCI.1327-18.2018>.
- Moran, A., Stein, E., Tischler, H., Belevsky, K., Bar-Gad, I., 2011. Dynamic stereotypic responses of basal ganglia neurons to subthalamic nucleus high-frequency stimulation in the parkinsonian primate. *Front. Syst. Neurosci.* 5, 21. <https://doi.org/10.3389/fnys.2011.00021>.
- Muthuraman, M., Koirala, N., Ciolac, D., Pinteá, B., Glaser, M., Groppa, Stanislav, Tamás, G., Groppa, Sergiu, 2018. Deep brain stimulation and L-DOPA therapy: concepts of action and clinical applications in Parkinson's disease. *Front. Neurol.* 9, 711. <https://doi.org/10.3389/fneur.2018.00711>.
- Neumann, W.-J., Degen, K., Schneider, G.-H., Brücke, C., Huebl, J., Brown, P., Kühn, A.A., 2016. Subthalamic synchronized oscillatory activity correlates with motor impairment in patients with Parkinson's disease. *Mov. Disord.* 31, 1748–1751. <https://doi.org/10.1002/mds.26759>.
- Okun, M.S., 2012. Deep-brain stimulation for Parkinson's disease. *N. Engl. J. Med.* 367, 1529–1538. <https://doi.org/10.1056/NEJMc1208070>.
- Oostenveld, R., Fries, P., Maris, E., Schoffelen, J., 2011. FieldTrip: Open Source Software for Advanced Analysis of MEG, EEG, and Invasive Electrophysiological Data. 2011 <https://doi.org/10.1155/2011/156869>.
- Oswal, A., Brown, P., Litvak, V., 2013. Synchronized neural oscillations and the pathophysiology of Parkinson's disease. *Curr. Opin. Neurol.* 26, 662–670. <https://doi.org/10.1097/WCO.0b000000000000034>.
- Özkurt, T.E., Butz, M., Homburger, M., Elben, S., Vesper, J., Wojtecki, L., Schnitzler, A., 2011. High frequency oscillations in the subthalamic nucleus: a neurophysiological marker of the motor state in Parkinson's disease. *Exp. Neurol.* 229, 324–331. <https://doi.org/10.1016/j.expneurol.2011.02.015>.
- Parsons, T.D., Rogers, S.A., Braaten, A.J., Woods, S.P., Tröster, A.I., 2006. Cognitive sequelae of subthalamic nucleus deep brain stimulation in Parkinson's disease: a meta-analysis. *Lancet Neurol.* 5, 578–588. [https://doi.org/10.1016/S1474-4422\(06\)70475-6](https://doi.org/10.1016/S1474-4422(06)70475-6).
- Quinn, E.J., Blumenfeld, Z., Velisar, A., Koop, M.M., Shreve, L.A., Trager, M.H., Hill, B.C., Kilbane, C., Henderson, J.M., Bronté-Stewart, H., 2015. Beta oscillations in freely moving Parkinson's subjects are attenuated during deep brain stimulation. *Mov. Disord.* 30, 1750–1758. <https://doi.org/10.1002/mds.26376>.
- Ramirez-Zamora, A., Giordano, J., Gunduz, A., Alcantara, J., Cagle, J.N., Cernera, S., Difuntorum, P., Eisinger, R.S., Gomez, J., Long, S., Parks, B., Wong, J.K., Chiu, S., Patel, B., Grill, W.M., Walker, H.C., Little, S.J., Gilroy, R., Tinkhauser, G., Thevathasan, W., Sinclair, N.C., Lozano, A.M., Foltynie, T., Fasanaro, A., Sheth, S.A., Scangos, K., Sanger, T.D., Miller, J., Brumback, A.C., Rajasethupathy, P., McIntyre, C., Schlachter, L., Suthana, N., Kubu, C., Sankary, L.R., Herrera-Ferrá, K., Goetz, S., Cheeran, B., Steinke, G.K., Hess, C., Almeida, L., Deeb, W., Foote, K.D., Okun, M.S., 2020. Proceedings of the seventh annual deep brain stimulation think tank: advances in neurophysiology, adaptive DBS, virtual reality, Neuroethics and technology. *Front. Hum. Neurosci.* 14, 54. <https://doi.org/10.3389/fnhum.2020.00054>.
- Rizzoli, S.O., Betz, W.J., 2005. Synaptic Vesicle Pools. <https://doi.org/10.1038/nrn1583>.
- Rosa, M., Arlotti, M., Marceglia, S., Cogiamanian, F., Ardolino, G., Di Fonzo, A., Lopiano, L., Scelzo, E., Merola, A., Locatelli, M., Rampini, P.M., Priori, A., 2017. Adaptive deep brain stimulation controls levodopa-induced side effects in Parkinsonian patients. *Mov. Disord.* <https://doi.org/10.1002/mds.26953>.
- Rosenbaum, R., Zimnik, A., Zheng, F., Turner, R.S., Alzheimer, C., Doiron, B., Rubin, J.E., 2014. Axonal and synaptic failure suppress the transfer of firing rate oscillations, synchrony and information during high frequency deep brain stimulation. *Neurobiol. Dis.* 62, 86–99. <https://doi.org/10.1016/j.nbd.2013.09.006>.
- Schiff, S.J., 2005. Dangerous phase. *Neuroinformatics* 3, 315–318. <https://doi.org/10.1385/NI:3:4:315>.
- Schneggenburger, R., Sakaba, T., Neher, E., 2002. Vesicle pools and short-term synaptic depression: lessons from a large synapse. *Trends Neurosci.* 25, 206–212. [https://doi.org/10.1016/S0166-2236\(02\)02139-2](https://doi.org/10.1016/S0166-2236(02)02139-2).
- Shivitz, N., Koop, M.M., Fahimi, J., Heit, G., Bronte-Stewart, H.M., 2006. Bilateral subthalamic nucleus deep brain stimulation improves certain aspects of postural control in Parkinson's disease, whereas medication does not. *Mov. Disord.* 21, 1088–1097. <https://doi.org/10.1002/mds.20905>.
- Sinclair, N.C., McDermott, H.J., Bulluss, K.J., Fallon, J.B., Perera, T., Xu, S.S., Brown, P., Thevathasan, W., 2018. Subthalamic nucleus deep brain stimulation evokes resonant neural activity. *Ann. Neurol.* 83, 1027–1031. <https://doi.org/10.1002/ana.25234>.
- Sinclair, N.C., Fallon, J.B., Bulluss, K.J., Thevathasan, W., 2019a. On the neural basis of deep brain stimulation evoked resonant activity. *Neurobiol. Dis.* 130, 104522. <https://doi.org/10.1016/j.nbd.2019.104522>.
- Sinclair, N.C., McDermott, H.J., Fallon, J.B., Perera, T., Brown, P., Bulluss, K.J., Thevathasan, W., 2019b. Deep brain stimulation for Parkinson's disease modulates high-frequency evoked and spontaneous neural activity. *Neurobiol. Dis.* 130, 104522. <https://doi.org/10.1016/j.nbd.2019.104522>.
- Slater, K.D., Sinclair, N.C., Nelson, T.S., Blamey, P.J., McDermott, H.J., 2015. neuroBi: a highly configurable Neurostimulator for a retinal prosthesis and other applications. *IEEE J. Transl. Eng. Heal. Med.* 3, 3800111. <https://doi.org/10.1109/JTEHM.2015.2455507>.
- Steiner, L.A., Barreda Tomás, F.J., Planert, H., Alle, H., Vida, I., Geiger, J.R.P., 2019. Connectivity and dynamics underlying synaptic control of the subthalamic nucleus. *J. Neurosci.* 39, 2470–2481. <https://doi.org/10.1523/JNEUROSCI.1642-18.2019>.
- Temperli, P., Ghika, J., Villemure, J.-G., Burkhard, P.R., Bogousslavsky, J., Vingerhoets, F.J.G., 2003. How do parkinsonian signs return after discontinuation of subthalamic DBS? *Neurology* 60, 78–81. <https://doi.org/10.1212/wnl.60.1.78>.
- Thevathasan, W., Sinclair, N.C., Bulluss, K.J., McDermott, H.J., 2020. Tailoring subthalamic nucleus deep brain stimulation for Parkinson's disease using evoked resonant neural activity. *Front. Hum. Neurosci.* 14, 71. <https://doi.org/10.3389/fnhum.2020.00071>.
- Tinkhauser, G., Pogoyan, A., Little, S., Beudel, M., Herz, D.M., Tan, H., Brown, P., 2017a. The modulatory effect of adaptive deep brain stimulation on beta bursts in Parkinson's disease. pp. 1053–1067. <https://doi.org/10.1093/brain/awx010>.
- Tinkhauser, G., Pogoyan, A., Tan, H., Herz, D.M., Kuhn, A.A., Brown, P., 2017b. Beta burst dynamics in Parkinson's disease OFF and ON dopaminergic medication. *Brain* 140, 2968–2981. <https://doi.org/10.1093/brain/awx252>.
- Tinkhauser, G., Pogoyan, A., Debove, I., Nowacki, A., Shah, S.A., Seidel, K., Tan, H., Brittain, J., Petermann, K., di Biase, L., Oertel, M., Pollo, C., Brown, P., Schuepbach, M., 2018. Directional local field potentials: a tool to optimize deep brain stimulation. *Mov. Disord.* 33, 159–164. <https://doi.org/10.1002/mds.27215>.
- Tinkhauser, G., Torrecillos, F., Pogoyan, A., Mostofi, A., Bange, M., Fischer, P., Tan, H., Hasegawa, H., Glaser, M., Muthuraman, M., Groppa, S., Ashkan, K., Pereira, E.A., Brown, P., 2020. The cumulative effect of transient synchrony states on motor performance in Parkinson's disease. *J. Neurosci.* 40, 1571–1580. <https://doi.org/10.1523/JNEUROSCI.1975-19.2019>.
- Torrecillos, F., Tinkhauser, G., Fischer, P., Green, A.L., Aziz, T.Z., Foltynie, T., Limousin, P., Zrinzo, L., Ashkan, K., Brown, P., Tan, H., 2018. Modulation of Beta bursts in the subthalamic nucleus predicts motor performance. *J. Neurosci.* 38, 8905–8917. <https://doi.org/10.1523/JNEUROSCI.1314-18.2018>.
- Vaillancourt, D.E., Prodoehl, J., Sturman, M.M., Bakay, R.A.E., Metman, L.V., Corcos, D.M., 2006. Effects of deep brain stimulation and medication on strength, bradykinesia, and electromyographic patterns of the ankle joint in Parkinson's disease. *Mov. Disord.* 21, 50–58. <https://doi.org/10.1002/mds.20672>.
- Velisar, A., Syrkin-Nikolaou, J., Blumenfeld, Z., Trager, M.H., Afzal, M.F., Prabhakar, V., Bronte-Stewart, H., 2019. Dual threshold neural closed loop deep brain stimulation in Parkinson disease patients. *Brain Stimul.* 12, 868–876. <https://doi.org/10.1016/j.brs.2019.02.020>.
- Waldvogel, D., Baumann-Vogel, H., Stieglitz, L., Hänggi-Schickli, R., Baumann, C.R., 2020. Beware of deep water after subthalamic deep brain stimulation. *Neurology* 94,

- 39–41. <https://doi.org/10.1212/WNL.0000000000008664>.
- Walker, H.C., Huang, H., Gonzalez, C.L., Bryant, J.E., Killen, J., Cutter, G.R., Knowlton, R.C., Montgomery, E.B., Guthrie, B.L., Watts, R.L., 2012. Short latency activation of cortex during clinically effective subthalamic deep brain stimulation for Parkinson's disease. *Mov. Disord.* 27, 864–873. <https://doi.org/10.1002/mds.25025>.
- Whitmer, D., de Solages, C., Hill, B., Yu, H., Henderson, J.M., Bronte-Stewart, H., 2012. High frequency deep brain stimulation attenuates subthalamic and cortical rhythms in Parkinson's disease. *Front. Hum. Neurosci.* 6, 155. <https://doi.org/10.3389/fnhum.2012.00155>.
- Wilson, C.J., Beverlin II, B., Netoff, T., 2011. Chaotic desynchronization as the therapeutic mechanism of deep brain stimulation. *Front. Syst. Neurosci.* 5, 50. <https://doi.org/10.3389/fnsys.2011.00050>.
- Wolf, M.E., Capelle, H.H., Bätzner, H., Hennerici, M.G., Krauss, J.K., Blahak, C., 2016. Hypokinetic gait changes induced by bilateral pallidal deep brain stimulation for segmental dystonia. *Gait Posture* 49, 358–363. <https://doi.org/10.1016/j.gaitpost.2016.07.301>.
- Yoshida, F., Martinez-Torres, I., Pogosyan, A., Holl, E., Petersen, E., Chen, C.C., Foltynie, T., Limousin, P., Zrinzo, L.U., Hariz, M.I., Brown, P., 2010. Value of subthalamic nucleus local field potentials recordings in predicting stimulation parameters for deep brain stimulation in Parkinson's disease. *J. Neurol. Neurosurg. Psychiatry* 81, 885–889. <https://doi.org/10.1136/jnnp.2009.190918>.
- Zaidel, A., Spivak, A., Shpigelman, L., Bergman, H., Israel, Z., 2009. Delimiting subterritories of the human subthalamic nucleus by means of microelectrode recordings and a hidden Markov model. *Mov. Disord.* 24, 1785–1793. <https://doi.org/10.1002/mds.22674>.